THE DUAL DOUBLE SCROLL EQUATION

by

Thomas S. Parker and Leon O. Chua

Memorandum No. UCB/ERL M86/99

1 August 1986

THE DUAL DOUBLE SCROLL EQUATION

by

Thomas S. Parker and Leon O. Chua

Memorandum No. UCB/ERL M86/99

1 August 1986

ELECTRONICS RESEARCH LABORATORY

College of Engineering
University of California, Berkeley
94720

TITLE PAGE

THE DUAL DOUBLE SCROLL EQUATION

by

Thomas S. Parker and Leon O. Chua

Memorandum No. UCB/ERL M86/99

1 August 1986

ELECTRONICS RESEARCH LABORATORY

College of Engineering
University of California, Berkeley
94720

The Dual Double Scroll Equation

Thomas S. Parker and Leon O. Chua

Department of Electrical Engineering and Computer Sciences,

University of California, Berkeley

ABSTRACT

This paper extends the Poincaré half-map technique, developed for the double scroll equation, in order to analyze the quite different dynamics of the dual double scroll equation. Two new uses of the Poincaré half-maps are presented: they are used to locate the boundaries between the return/transfer/escape regions and to detect a period-one limit cycle. The Poincaré half-map technique is also used to detect homoclinic and heteroclinic orbits and to locate the region in parameter space for which stable attracting sets exist.

1. Introduction

Recently, a powerful technique utilizing Poincaré half-maps was developed for the analysis of third-order piecewise-linear ordinary differential equations [1]. The technique is applicable to two large families of PWL ODEs: the double scroll family and the dual double scroll family. The double scroll equation [2]—one member of the double scroll family—initially motivated the research and has been analyzed in depth in [1]. The purpose of this paper is to extend the Poincaré half-map technique to perform an analysis on a typical member of the dual double scroll family, namely, the dual double scroll equation, and to introduce two new uses for the Poincaré half-maps: they are used to locate the boundaries of the return/transfer/escape regions and to detect the existence and position of a period-one limit cycle. Though our analysis is performed on a specific equation, the techniques presented here have broad applicability in the study of PWL ODEs. For example, the techniques can be applied directly to the feedback system presented by Sparrow in [3] since it is a member of the dual double scroll family.

Research supported in part by the Hertz Foundation, by the Office of Naval Research under Contract N00014-86-K-0351 and by National Science Foundation Grant ECS8313278.

The dual double scroll equation—and, therefore, the dual double scroll family—derives its name from the fact that it describes the same circuit as the double scroll equation except for the single nonlinear element which is the dual of the double scroll nonlinearity. Although the dual double scroll equation is closely related to the double scroll equation, its dynamic behavior is quite different.

In Section 2, computer simulations are used to familiarize the reader with the qualitative behavior of the dual double scroll equation. In Section 3, notation is defined and a brief review of the pertinent portions of [1] is presented. In Section 4, the Poincaré half-maps are defined in a more general fashion than is done in [1]: no assumptions are made on the system dynamics and they are defined with the largest possible domain. These more general definitions are used in Section 5 to locate the return/transfer/escape boundaries. In Section 6, the existence of homoclinic and heteroclinic orbits is demonstrated while the set of parameters for which there exists a stable attracting set is derived in Section 7. Finally, in Section 8, the Poincaré half-maps are used to show the existence of a period-one limit cycle.

2. The Dual Double Scroll Equation

The PWL ODE examined in this paper is

$$\begin{aligned} \dot{x} &= \alpha(y - h(x)) \\ \dot{y} &= x - y + z \\ \dot{z} &= -\beta y \end{aligned} \tag{1}$$

where the piecewise-linearity is

$$h(x) := m_1 x + \frac{m_0 - m_1}{2}(|x + 1| - |x - 1|). \tag{2}$$

The piecewise-linearity $h(x)$ divides the state space $\mathbb{R}^3$ into three regions: $x < -1$, $-1 < x < 1$ and $x > 1$. In each region, (1) reduces to a linear system. Throughout out this paper, the slopes m_0 and m_1 are fixed at $m_0 = 2/7$ and $m_1 = -1/7$. This PWL ODE is the dimensionless form of the double scroll equation ((1.1) and (1.2) of [1]) with the values of m_0 and m_1 switched. It will be seen to have many similarities to and several differences from the double scroll equation.

To give the reader a feeling for the types of behavior encountered in the dual double scroll equation, the results of a series of computer simulations of (1) with $\alpha = 9$ are presented in Fig. 1. As β is

varied, the steady-state solution demonstrates a variety of behavior including Hopf bifurcation, period doubling, chaos and periodic windows.

For $\beta > 23$, the origin is a stable equilibrium point. As β decreases below 23, the complex eigenvalues at the origin pass through the $j\omega$ axis and a Hopf bifurcation occurs. The stable equilibrium point becomes unstable and a stable symmetric limit cycle—passing through all three regions of the state space—appears (Fig. 1(a)). This behavior differs from the Hopf bifurcation of the double scroll where the limit cycle is not odd symmetric and is confined to two of the three regions.

As β decreases, this symmetric limit cycle becomes larger in diameter. At approximately $\beta = 15$, it becomes asymmetric (Fig. 1(b)). The odd symmetry of (1) implies the existence of a second limit cycle—identical to the first, but reflected through the origin.

By $\beta = 13.8$, the limit cycle has doubled in period (Fig. 1(c)) and by $\beta = 13.7$, it has period-doubled again. For $\beta = 13.6$, the steady state is still asymmetric but is now chaotic (Fig. 1(d)). As β decreases further, the chaotic steady state grows in diameter until at $\beta = 13.5$, the asymmetric steady state appears to have joined with its twin and the steady-state chaos becomes symmetric (Fig. 1(e)). This sequence is similar to the birth of the double scroll attracting set described in [1] except that for the double scroll, the asymmetric chaos is confined to two regions while for the dual double scroll equation, the chaotic trajectory passes through all three regions.

At $\beta = 13.28$, there is a period five limit cycle (Fig. 1(f)) and for $\beta = 13.1$, chaos has returned. For $\beta < 12.8$, there is no observable steady-state behavior as all simulations become unbounded.

3. Definitions, Notation and Review

Powerful machinery for the analysis of a large family of third-order PWL ODEs has been developed in [1]. In this section, the pertinent parts of that paper are quickly reviewed. The interested reader is strongly urged to refer to [1] for a more complete discussion.

Nearly identical notation is used as in [1], so the reader familiar with [1] may skip this section.

3.1. Mathematical notation

$\overline{XY}$ is the line segment with endpoints X and Y.

$\overrightarrow{XY}$ is the ray from X through Y.

$\overleftrightarrow{XY}$ is the line through X and Y.

XY is the curve joining X and Y.

$\square X_1 \ldots X_n$ is the region whose boundary contains the points $X_1, \ldots, X_n$. The actual boundary will be clear from looking at the particular figure referenced.

$\bar{S}$ is the closure of the set S.

No special convention is used to distinguish between vectors and scalars; the meaning will be clear by context.

3.2. The vector field

The techniques developed in [1] apply to a vector field $\xi : \mathbb{R}^3 \to \mathbb{R}^3$ that satisfies the following six properties (see Fig. 2):

(P.1) ξ is symmetric with respect to the origin.

(P.2) There are two parallel planes U_1 and U_{-1}, that partition $\mathbb{R}^3$ into three regions D_{-1}, D_0 and D_1. (P.1) implies $U_1 = -U_{-1}$.

(P.3) In each region D_i, $(i = -1, 0, 1)$, ξ is affine; that is, $D\xi(\hat{x}) = M_i$ for $\hat{x} \in D_i$ where $M_i \in \mathbb{R}^{3\times 3}$. (P.1) implies that $M_1 = M_{-1}$.

(P.4) ξ has three equilibrium points, one at the origin labeled P_0, one in D_1 labeled P_1 and one in D_{-1} labeled P_{-1}. (P.1) implies that $P_1 = -P_{-1}$. Note that in [1], P_1 is labeled P^+ and P_{-1} is P^-.

(P.5) Associated with each equilibrium point P_i, $(i = -1, 0, 1)$, is a real eigenvalue $\tilde{\gamma}_i \neq 0$ and a pair of complex conjugate eigenvalues $\tilde{\sigma}_i \pm j\tilde{\omega}_i$ where $\tilde{\omega}_i > 0$. (P.1) implies $\tilde{\sigma}_1 = \tilde{\sigma}_{-1}$, $\tilde{\omega}_1 = \tilde{\omega}_{-1}$ and $\tilde{\gamma}_1 = \tilde{\gamma}_{-1}$. Within each region, the eigenvector associated with the real eigenvalue is called the *real eigenvector* and the plane spanned by the real and imaginary parts of

the eigenvector associated with the complex conjugate eigenvalues is called the *eigenplane*.

(P.6) For P_i, ($i = -1, 0, 1$), neither the real eigenvector nor the eigenplane is parallel to U_1 or U_{-1}.

3.3. Double scroll versus dual double scroll

The *double scroll family* is the set of all PWL ODEs that satisfy properties (P.1) through (P.6) and that have $\bar{\gamma}_0 > 0$ and $\bar{\gamma}_1 < 0$. The *dual double scroll family* is the set of all PWL ODEs that satisfy the six properties and that have $\bar{\gamma}_0 < 0$ and $\bar{\gamma}_1 > 0$.

There are six parameters ($\bar{\sigma}_0$, $\bar{\omega}_0$, $\bar{\gamma}_0$, $\bar{\sigma}_1$, $\bar{\omega}_1$ and $\bar{\gamma}_1$) needed to distinguish between members of the dual double scroll family. The dual double scroll equation has only two parameters (α and β). It follows that the dual double scroll equation is a very small subset (measure zero) of the dual double scroll family. The techniques presented in this paper apply to the entire dual double scroll family and, therefore, have much broader applicability than to just (1).

The interesting behavior in both the double scroll equation and the dual double scroll equation occurs when each equilibrium point possesses *contracting and expanding* directions ($\bar{\sigma}_i \bar{\gamma}_i < 0$) and this is the case considered in this paper. It follows that *the equilibrium points of the dual double scroll equation have the opposite stability behavior as those of the double scroll*.

Since the (real parts of the) eigenvalues of the dual double scroll family have signs opposite those of the double scroll family, the dual double scroll family can be thought of as the double scroll family *in reverse time*. This interpretation will be instrumental in extending the techniques of [1]—specifically formulated for the double scroll family—to the dual double scroll family.

3.4. Strategic points

There are six points of interest located on U_1 called *strategic points*.

$A \in U_1$ is the point of intersection of the eigenplane in D_1 and the eigenplane in D_0.

$C \in U_1$ is the point where the D_0 real eigenvector intersects U_1.

$D \in U_1$ is the point where the D_1 real eigenvector intersects U_1.

$\overleftrightarrow{EB} \subset U_1$ is the line such that $\xi(\hat{x})$ is tangent to U_1 for all $\hat{x} \in \overleftrightarrow{EB}$. B is chosen on the D_1

eigenplane and E on the D_0 eigenplane.

$F \in \overleftrightarrow{EB}$ is the point such that $\xi(F)$ is parallel to $\overleftrightarrow{EB}$.

3.5. The D_1 and D_0 units

There exists an affine map, $\Psi_1 : \mathbb{R}^3 \to \mathbb{R}^3$ that maps D_1 into the D_1 unit (Fig. 2). In the D_1 unit, the origin is the equilibrium point, the eigenplane is the x-y plane; the real eigenvector is the z axis; U_1 becomes the plane $V_1 = \{(x, y, z,) \mid x + z = 1\}$;[1] the strategic points map to A_1, B_1, C_1, D_1, E_1 and F_1 (formulae for these points in terms of the eigenvalues are given in [1]); and the vector field assumes the real Jordan form

$$\begin{bmatrix} \dot{x} \\ \dot{y} \\ \dot{z} \end{bmatrix} = \begin{bmatrix} \sigma_1 & -1 & 0 \\ 1 & \sigma_1 & 0 \\ 0 & 0 & \gamma_1 \end{bmatrix} \begin{bmatrix} x \\ y \\ z \end{bmatrix} \tag{3}$$

where $\sigma_1 := \bar{\sigma}_1/\bar{\omega}_1$ and $\gamma_1 := \bar{\gamma}_1/\bar{\omega}_1$. The solution to (3) passing through $\hat{x}$ at time $t = 0$ is denoted $\phi_1^t(\hat{x})$. In the D_1 unit, the eigenplane is stable and the real eigenvector is unstable. A typical trajectory spirals in around the z axis and grows exponentially out in the z direction.

Likewise, there is a linear transformation Ψ_0 that maps D_0 into the D_0 unit (Fig. 2). The geometry of the D_0 unit is analogous to that of the D_1 unit except that there are two boundary planes: V_0 corresponds to U_1 and $V_0^- = \{(x, y, z,) \mid x + z = -1\}$ corresponds to U_{-1}. The flow in the D_0 unit is

$$\begin{bmatrix} \dot{x} \\ \dot{y} \\ \dot{z} \end{bmatrix} = \begin{bmatrix} \sigma_0 & -1 & 0 \\ 1 & \sigma_0 & 0 \\ 0 & 0 & \gamma_0 \end{bmatrix} \begin{bmatrix} x \\ y \\ z \end{bmatrix} \tag{4}$$

where $\sigma_0 := \bar{\sigma}_0/\bar{\omega}_0$ and $\gamma_0 := \bar{\gamma}_0/\bar{\omega}_0$. The solution to (4) that passes through $\hat{x}$ at time $t = 0$ is denoted $\phi_0^t(\hat{x})$. The eigenplane is unstable and the real eigenvector is stable—just the opposite to the D_1 unit. A typical trajectory collapses toward the eigenplane while spiraling outward away from the origin.

Since the D_1 and D_0 units use different coordinate systems, there exists an affine connection map $\Phi : V_0 \to V_1$ that maps coordinates on the upper boundary of the D_0 unit to the boundary in the D_1

[1] We use (x, y, z) for both the original vector space and the D_1 unit. The meaning will be clear by context.

unit.

All the analysis in this paper will be carried out in the D_1 and D_0 units.

4. Poincaré Half-maps

In this section, the Poincaré map (first return map) π is defined for the dual double scroll family and a method for calculating it analytically is also presented. π will be defined in terms of two half-maps: π_0 and π_1. π_0 is the first return map for the D_0 unit and π_1 is the first return map for the D_1 unit. We define the half-maps in a more general fashion than is done in [1] by making no assumptions on the system dynamics and by increasing the domain of each half-map to the largest possible set.

First, some definitions are in order. $\hat{x} \in V_i$, $(i = 0, 1)$, is a D_i *entry point* if there exists a $\hat{t} > 0$ such that $\phi_i^t(\hat{x})$ lies in the D_i unit for all $0 < t < \hat{t}$. If $\hat{x} \in V_i$ is not a D_i entry point, it is called a D_i *exit point*.

Let V_i^{in}, $(i = 0, 1)$, be the set of all D_i entry points. Let $V_i^{out} = V_i \setminus V_i^{in}$, $(i = 0, 1)$, be the set of all D_i exit points. If $\hat{x}$ is a D_0 (D_1) entry point, then $\Phi(\hat{x})$ ($\Phi^{-1}(\hat{x})$) is a D_1 (D_0) exit point, that is, $V_1^{in} = \Phi(V_0^{out})$ and $V_1^{out} = \Phi(V_0^{in})$.

$\overleftrightarrow{EB}$ divides U_1 into two half-planes. On one half-plane, ξ points into D_0; on the other, ξ points into D_1. On $\overleftrightarrow{EB}$ itself, ξ is tangent to U_1 and, therefore, all trajectories incident to $\overleftrightarrow{EB}$ are tangent to U_1. The ray $\overrightarrow{FE}$ consists of points where trajectories are tangent from D_0 while $\overrightarrow{FB}$ consists of points where the trajectory is tangent from D_1. Hence, V_0^{in} consists of the union of the ray $\overrightarrow{F_0E_0}$ with all points of V_0 above $\overleftrightarrow{E_0B_0}$ (i.e., on the side opposite A_0) and V_1^{in} consists of the union of the ray $\overrightarrow{F_1B_1}$ with all points of V_1 below $\overleftrightarrow{E_1B_1}$ (i.e., on the same side as A_1).

4.1. Definition of π_1

Given $\hat{x} \in V_1^{in}$, the trajectory $\phi_1^t(\hat{x})$ emanating from $\hat{x}$ will do one of three things:

a) Hit the boundary V_1 at some time $t \geq 0$;

b) Never touch V_1 and, remaining in the D_1 unit for all $t > 0$, approach the equilibrium point (i.e., the origin) as $t \to \infty$.

c) Never touch V_1 and, remaining in the D_1 unit for all $t > 0$, become unbounded as $t \to \infty$. This behavior cannot occur for the double scroll family and is a major difference between the dual double scroll equation and the double scroll.

Points of type a) and b) are called *return points* while type c) points are called *escape points*. Define $R_1 \subset V_1^{in}$ as the set of return points for the D_1 unit. R_1 will be precisely determined in Section 5.1.

$\pi_1 : \overline{R_1} \to \overline{V_1^{out}}$ is defined for the dual double scroll family much as it is for the double scroll family, but *in forward time*. Given $\hat{x} \in \overline{R_1}$, $\pi_1(\hat{x})$ is the point where the trajectory emanating from $\hat{x}$ first returns to V_1. It is convenient to define $\hat{\pi}_1 : \overline{R_0} \to \overline{V_0^{in}}$ by $\hat{\pi}_1 := \Phi^{-1} \circ \pi_1 \circ \Phi$ where $R_0 := \Phi^{-1}(R_1)$. $\hat{\pi}_1$ is simply π_1 transferred to the D_0 unit coordinate system.

Any point on V_1 is uniquely determined by its x and y coordinates so the z coordinate ($= 1 - x$) will be suppressed. It will be useful to define nonlinear u-v coordinates on V_1^{in}:

$$\tilde{x}_1(u, v) = u[vA_1 + (1 - v)E_1] + (1 - u)[vB_1 + (1 - v)F_1]. \tag{5}$$

Note that the set of D_1 entry points $V_1^{in} = \{(u, v) \mid u > 0, v \geq 0\}$ and that $\overline{R_1}$ is some subset of $\overline{V_1^{in}} = \{(u, v) \mid u \geq 0, v \geq 0\}$

Calculation of π_1:

Let $\hat{x} \in \overline{R_1}$ have x-y coordinates (x, y) and u-v coordinates (u, v).

i) Calculate the inverse return-time function

$$v(u, t) := \begin{cases} \dfrac{<\phi_1^t(E_{1u}), h> - 1}{<\phi_1^t(E_{1u} - A_{1u}), h>} & t > 0 \\ 0 & t = 0 \end{cases} \tag{6}$$

where $E_{1u} := \tilde{x}_1(u, 0)$, $A_{1u} := \tilde{x}_1(u, 1)$ and $h := [1\ 0\ 1]^T$ is the normal vector to V_1. $v(u, t) = 0$ as $t \to 0$ as can be shown by L'Hopitâl's rule; hence, $v(u, 0)$ is defined to be 0.

ii) Use v to calculate the first return time

$$\hat{t} := \min\{t \geq 0 \mid v(u, t) = v\}. \tag{7}$$

iii) Then the Poincaré half-map π_1 is given by

$$\pi_1(\hat{x}) := \begin{cases} e^{\sigma_1 \hat{t}} \begin{bmatrix} \cos\hat{t} & -\sin\hat{t} \\ \sin\hat{t} & \cos\hat{t} \end{bmatrix} \begin{bmatrix} x \\ y \end{bmatrix} & \text{if } \hat{t} \text{ exists,} \\ D_1 & \text{otherwise.} \end{cases} \tag{8}$$

4.2. Discussion of π_1

Given a coordinate u and a time t, the inverse return-time function $v(u, t)$ gives the v coordinate such that the trajectory emanating from $(u, v(u, t))$ intersects the boundary V_1 in t seconds *assuming the* D_1 *dynamics have been extended to all of* $\mathbb{R}^3$. A proof is presented in [1].

For a given (u, v) there are two cases:

1) $v(u, t) \neq v$ for all $t \geq 0$. Hence, the trajectory from (u, v) never leaves the D_1 unit. If such a trajectory becomes unbounded, (u, v) is an escape point and $\pi_1(\tilde{x}_1(u, v))$ is not well-defined. If the trajectory does not become unbounded, (u, v) must lie on the eigenplane (i.e., $v = 1$) and the trajectory must approach the origin of the D_1 unit. In this case, $\pi_1(\tilde{x}_1(u, v))$ is defined to be equal to the fundamental point D_1 and (u, v) is a return point.

2) $v(u, t) = v$ for some value of $t = t'$. In this case, $\pi_1(\tilde{x}_1(u, v))$ is well-defined and (u, v) is a return point. If $v(u, t) = v$ for more than one time t, the minimum value of t is the first return time. All other t values are *virtual return times* caused by the extension of the D_1 dynamics to all of $\mathbb{R}^3$; they are not physically meaningful.

In practice, π_1 is calculated for a line u = constant since $v(u, t)$ yields all the first return times for a given value of u. Fig. 3(a) shows $\pi_1(\overrightarrow{F_1B_1})$ (i.e., $u = 0$) and $\pi_1(\overrightarrow{E_1A_1})$ (i.e., $u = 1$) for $\alpha = 9$ and $\beta = 15$. Notice that both images are spirals winding around the point D_1. The functions $v(0, t)$ and $v(1, t)$ are both monotone increasing from $v = 0$ to $v = 1$. $v(0, t)$ is shown in Fig. 3(b); $v(1, t)$ looks qualitatively the same. The fact that $v(0, t) < 1$ for all $t > 0$ implies that $\overline{E_1A_1}$ consists of return points while $\overrightarrow{A_1A_{1\infty}}$ is composed of escape points. Likewise, $\overline{F_1B_1}$ consists of return points while escape points comprise $\overrightarrow{B_1B_{1\infty}}$. The points A_1 and B_1 are mapped into the point D_1 by π_1; in fact, for this example, all points in $\overline{B_1A_1}$ map to D_1. Also note that F_1 and E_1 are fixed points of π_1; indeed,

$v(u, 0) = 0$ implies that every point in $\overrightarrow{F_1E_1}$ is a fixed point of π_1 and that these are the only fixed points.

The behavior of π_1 is similar for other values of u between 0 and 1. Hence, the triangle $\square A_1B_1E_1$ maps into the spiraling snake $\square F_1E_1D_1$. If u is increased beyond 1, the spiral behavior of π_1 continues until some u is reached such that $\pi_1(\overline{E_{1u}A_{1u}})$ is no longer a spiral. Though this behavior will not be of interest for π_1, it will be examined when π_0 is discussed.

4.3. Definition of π_0

$\pi_0 : \overline{V_0^{out}} \rightarrow \overline{V_0^{in}}$ is defined for the dual double scroll family much as it is for the double scroll family, but *in reverse time* which explains why the domain is the set of D_0 *exit* points and the range is the set of D_0 *entry* points. It is convenient to define $\hat{\pi}_0 : \overline{V_1^{in}} \rightarrow \overline{V_1^{out}}$ by $\hat{\pi}_0 := \Phi \circ \pi_0 \circ \Phi^{-1}$. $\hat{\pi}_0$ is simply π_0 transferred to the D_1 unit coordinate system.

π_0 has two parts: π_0^+ characterizes trajectories that return to V_0 and π_0^- characterizes those that cross to V_0^-.

Any point on V_0 is uniquely determined by its x and y coordinates so the z coordinate will be suppressed. Define nonlinear u-v coordinates on V_0^{out}:

$$\tilde{x}_0(u, v) = u[vA_0 + (1 - v)E_0] + (1 - u)[vB_0 + (1 - v)F_0]. \tag{9}$$

Note that $V_0^{out} = \{(u, v) \mid u > 0, v \geq 0\}$ while $\overline{V_0^{out}} = \{(u, v) \mid u \geq 0, v \geq 0\}$.

Calculation of π_0:

Let $\hat{x} \in \overline{V_0^{out}}$ have x-y coordinates (x, y) and u-v coordinates (u, v).

i) Calculate the V_0 inverse return-time function

$$u^+(v, t) := \begin{cases} \dfrac{\langle \phi_0^{-t}(B_{0v}), h \rangle - 1}{\langle \phi_0^{-t}(B_{0v} - A_{0v}), h \rangle} & t > 0 \\ 0 & t = 0 \end{cases} \tag{10}$$

and the V_0^- inverse return-time function

$$u^-(v, t) := \frac{\langle \phi_0^{-t}(B_{0v}), h \rangle + 1}{\langle \phi_0^{-t}(B_{0v} - A_{0v}), h \rangle} \qquad t > 0 \tag{11}$$

where $B_{0v} := \tilde{x}_0(0, v)$, $A_{0v} := \tilde{x}_0(1, v)$ and $h := [1\ 0\ 1]^T$ is the normal vector to V_0.

$u^+(\nu, t) \to 0$ as $t \to 0$ as can be shown by L'Hopitâl's rule; hence, $u^+(\nu, 0)$ is defined to be 0.

ii) Define the V_0 first return time as

$$\hat{t}^+ := \min\{ t \geq 0 \mid u^+(t, \nu) = u \} \tag{12}$$

and the V_0^- first return time as

$$\hat{t}^- := \min\{ t \geq 0 \mid u^-(t, \nu) = u \}. \tag{13}$$

iii) If $\hat{t}^+$ exists, define the V_0 first return map

$$\pi_0^+(\hat{x}) := e^{-\sigma_0 \hat{t}^+} \begin{bmatrix} \cos(\hat{t}^+) & \sin(\hat{t}^+) \\ -\sin(\hat{t}^+) & \cos(\hat{t}^+) \end{bmatrix} \begin{bmatrix} x \\ y \end{bmatrix} \tag{14}$$

and, if $\hat{t}^-$ exists, define the V_0^- first return map

$$\pi_0^-(\hat{x}) := e^{-\sigma_0 \hat{t}^-} \begin{bmatrix} \cos(\hat{t}^-) & \sin(\hat{t}^-) \\ -\sin(\hat{t}^-) & \cos(\hat{t}^-) \end{bmatrix} \begin{bmatrix} x \\ y \end{bmatrix}. \tag{15}$$

iv) Then the Poincaré half-map π_0 is given by

$$\pi_0(\hat{x}) := \begin{cases} C_0 & \text{neither } \hat{t}^- \text{ nor } \hat{t}^+ \text{ exists,} \\ \pi_0^+(\hat{x}) & \hat{t}^+ < \hat{t}^- \text{ or } \hat{t}^- \text{ does not exist,} \\ -\pi_0^-(\hat{x}) & \hat{t}^- < \hat{t}^+ \text{ or } \hat{t}^+ \text{ does not exist.} \end{cases} \tag{16}$$

4.4. Discussion of π_0

We start by reiterating that π_0 is calculated for the flow in reverse time. Since the eigenvalues at the origin (P_0) have signs opposite those at P_1, the reverse dynamics in the D_0 unit are qualitatively similar to the forward dynamics in the D_1 unit. Thus, one would not expect π_0 to be too different from π_1.

The one major difference is that there are two boundaries, V_0 and V_0^-, associated with the D_0 unit. Given a coordinate ν and a time t, $u^+(\nu, t)$ gives the u coordinate such that the trajectory emanating from $(u^+(\nu, t), \nu)$ intersects the boundary V_0 in $-t$ seconds *assuming the* D_0 *dynamics have been extended to all of* $\mathbf{R}^3$.

Likewise, the trajectory emanating from $(u^-(\nu, t), \nu)$ intersects V_0^- in $-t$ seconds assuming the D_0 dynamics have been extended to all of $\mathbb{R}^3$.

A trajectory $\phi_0^{-t}(\hat{x})$ emanating (in reverse time) from a D_0 exit point $\hat{x}$ can do one of three things:

1) The trajectory can stay in the D_0 unit forever. This will happen only if the trajectory tends toward the origin. In this case, neither $\hat{t}^+$ nor $\hat{t}^-$ exists and $\pi_0(\hat{x})$ is defined to be C_0.

2) The trajectory can return to the boundary V_0. In this case, either $\hat{t}^+ < \hat{t}^-$ or $\hat{t}^-$ does not exist; in either event, $\pi_0(\hat{x}) = \pi_0^+(\hat{x})$. $\pi_0(\hat{x})$ is called a *return point* because the trajectory $\phi_0^t(\pi_0(\hat{x}))$ emanating (in forward time) from $\pi_0(\hat{x})$ returns to V_0.

3) The trajectory can cross the D_0 unit and hit V_0^-. In this case, either $\hat{t}^- < \hat{t}^+$ or $\hat{t}^+$ does not exist; in either event, $\pi_0(\hat{x}) = -\pi_0^-(\hat{x})$. The minus sign reflects π_0^- through the origin and is necessary since the range of π_0^- lies in V_0^- and the range of π_0 lies in V_0. The reflection produces no loss of information since (1) is odd symmetric. $\pi_0(\hat{x})$ is called a *transfer point* because the trajectory $\phi_0^t(\pi_0(\hat{x}))$ emanating from $\pi_0(\hat{x})$ does not return to V_0 but crosses over to V_0^-.

There is a certain duality between π_0 and π_1. If u and v are switched and B and E are switched and the y axis is inverted in either the D_0 or D_1 unit, then the two maps are qualitatively identical except for the fact that π_0 has to deal with two boundaries. For example, π_1 is calculated along lines of constant u, while π_0 is calculated for lines v = constant. For π_1, $\overrightarrow{F_1E_1}$ consists of fixed points while for π_0, $u^+(v, 0) = 0$ implies that all points in $\overrightarrow{F_0B_0}$ are fixed points and that these are the only fixed points. This duality is the main reason π_0 is defined in reverse time.

There is a simple criterion to determine whether a point is a transfer or return point: $\pi_0(\hat{x})$ is a return (transfer) point if $\hat{x}$ and $\pi_0(\hat{x})$ lie on the same side (on different sides) of the line $x = 1$; if both points lie on $x = 1$, then $\pi_0(\hat{x})$ is a transfer point. The key fact in the proof is that a trajectory cannot pass through the eigenplane. It follows that if the x coordinate of $\hat{x}$ is greater (less) than 1, then the x coordinate of $\pi_0^+(\hat{x})$ is greater (less) than 1 and the x coordinate of $\pi_0^-(\hat{x})$ is greater (less) than -1. If $\pi_0(\hat{x})$ is a return point, then $\pi_0(\hat{x}) = \pi_0^+(\hat{x})$ and the x coordinate of $\pi_0(\hat{x})$ is greater (less) than 1; if $\pi_0(\hat{x})$ transfers, then $\pi_0(\hat{x}) = -\pi_0^-(\hat{x})$ and the x coordinate of $\pi_0(\hat{x})$ is less (greater) than 1.

There are three typical types of π_0 behavior encountered in this paper which will be discussed one by one. All examples in this section are for $\alpha = 9$ and $\beta = 13$.

The simplest behavior is in Fig. 4(a) which shows $\pi_0(\overrightarrow{F_0E_0})$ (i.e., $v = 0$). $\pi_0(\overrightarrow{F_0E_0})$ consists of two spirals, each wrapping around C_0. $\pi_0(F_0) = F_0$ and $\pi_0(E_0) = C_0$ so the spiral F_0C_0 connecting F_0 and C_0 is $\pi_0(\overline{F_0E_0})$. $\overline{F_0E_0}$ and F_0C_0 both lie on the same side of the line $x = 1$ so F_0C_0 consists of return points. The other spiral $E'_{0-}C_0$ is $\pi_0(\overrightarrow{E_0E_{0-}})$. $E'_{0-}C_0$ and $\overrightarrow{E_0E_{0-}}$ lie on opposite sides of $x = 1$ and, therefore, $E'_{0-}C_0$ is composed of transfer points. This example corresponds to monotone increasing u^+ and monotone decreasing u^- with no overlapping of u^+ and u^-, that is, $u^+(v, t) < 1$ and $u^-(v, t) > 1$ for all $v, t > 0$ (Fig. 4(b)).

Fig. 5(a) shows $\pi_0(\overrightarrow{B_{0v}A_{0v}})$ for $v = 0.5$. $\pi_0(\overline{B_{0v}A_{0v}})$ maps to the spiral $B_{0v}C_0$ connecting B_{0v} and C_0; however, $\pi_0(\overrightarrow{A_{0v}A_{0v-}})$ touches $\overrightarrow{F_0E_0}$ and is broken into two pieces $A'_{0v-}Q'$ and $Q''C_0$. $B_{0v}C_0$ consists of return points while $A'_{0v-}Q'$ and $Q''C_0$ are composed of transfer points. This case corresponds to monotone increasing u^+, non-monotone u^- and no overlapping of u^+ and u^- (Fig. 5(b)). The non-monotonicity of u^- implies that there are *virtual return times* caused by the extension of the D_0 dynamics to all of $\mathbb{R}^3$. There are also *virtual return points* corresponding to these virtual return times. The points that would be needed to connect $\pi_0(\overrightarrow{A_{0v}A_{0v-}})$ into a single spiral are precisely these virtual return points.

To understand this split spiral behavior more fully, consider the magnified (and somewhat distorted) version of $u^-(0.5, t)$ shown in Fig. 6(a). Let t_1, t_2, t_3, u_1 and u_2 be defined as in the Figure. Figs. 6(b) through 6(f) show a typical trajectory of a two-dimensional system with two boundaries, U_{-1} and U_1, for each of five cases:[2]

a) $u > u_2$: There is only one return time; the crossing is transverse.

b) $u = u_2$: There are two return times; the first crossing is transverse and the second, at $t = t_2$, is tangent.

c) $u_1 < u < u_2$: There are three return times; all the crossings are transverse.

d) $u = u_1$: There are two return times; the first, at $t = t_1$ is tangent while the second, at $t = t_3$, is transverse.

[2] The trajectories pictured obviously cannot occur in a PWL autonomous ODE, but are abstractions used to illustrate the essential features.

e) $u < u_1$: There is only one return time and the crossing is transverse.

Note that a local minimum or maximum of u^- implies that the trajectory is tangent to the boundary at the return point. Such a return point must lie on $\overleftrightarrow{E_0B_0}$. Also note that, in going from case d) to case e), the first return time jumps from t_1 to t_3 implying a discontinuity in π_0. In Fig. 5(a), this discontinuity occurs at some point $Q \in \overrightarrow{A_{0v}A_{0v-}}$ with u-v coordinates $(u_1, 0.5)$; that is,

$$\lim_{\substack{u \to u_1 \\ u > u_1}} \pi_0(\tilde{x}_0(u, 0.5)) = Q' \tag{17}$$

and

$$\lim_{\substack{u \to u_1 \\ u < u_1}} \pi_0(\tilde{x}_0(u, 0.5)) = Q'' \ . \tag{18}$$

The trajectory $\phi_0^{-t}(Q)$ from Q first hits a boundary (V_0^-) at point Q' at time t_1 and, therefore, $\pi_0(Q) = Q'$. $Q' \in \overline{F_0E_0}$ so the trajectory is tangent to the boundary and does not leave the D_0 unit at this time. Instead, it continues until it next hits a boundary (V_0^-) at point Q'' at time t_3. It follows that $\pi_0(Q') = Q''$ with a return time $t_3 - t_1$.

Note that the trajectory $\phi_0^{-t}(Q)$ from Q does not *leave* the D_0 unit until it hits the point Q'' at $t = t_3$; however, $\pi_0(Q) = Q'$, not Q''. It appears that π_0 is ill-defined. This paradox will be resolved in Section 4.5.

The third case is shown in Fig. 7(a) which is a plot of $\pi_0(\overrightarrow{B_0A_0})$. There are two partial spirals, neither of which wraps around C_0. The key difference between this example and the previous two is that the upper spiral crosses the line $x = 1$ that corresponds to the intersection of V_0 with the eigenplane. $\pi_0(A_0) = A'$ since trajectories starting on the eigenplane must remain on it for all time. Thus $\pi_0(\overrightarrow{A_0A_{0-}})$ maps to $A'A'_{0-}$. There exists a point $Q \in \overline{B_0A_0}$ such that $\pi_0(\overline{QA_0})$ maps to $A'Q$ and $\pi_0(\overline{B_0Q})$ maps to B_0Q''. Return points comprise B_0Q'' while $A'_{0-}Q'$ consists of transfer points. This case corresponds to a monotone increasing u^+, a non-monotone u^- and an overlapping of u^+ and u^-. Fig. 7(b) is a magnified plot of u^+ and u^- for this example. The point $(u', 1)$ corresponds to Q. In t' seconds, the trajectory $\phi_0^{-t}(Q)$ starting at Q intersects V_0^- at $-Q'$;

in t'' seconds, it intersects V_0 at Q''. $\pi_0(\overrightarrow{B_0A_0})$ does not wrap around C_0 since for $t > t''$, all return times are virtual.

Finally, in Fig. 8 $\pi_0(\overrightarrow{B_{0\nu}A_{0\nu}})$ is plotted for several values of ν between 0 and $\nu' = 1.2$. This plot illustrates the fact that π_0 maps the wedge $\square E_{0-\infty}B_{0\nu}A_{0\nu'-\infty}$ *onto* the region $\square A'_{0\nu'-\infty}Q'B_{0\nu}Q''E'_{0-\infty}$, that is, there are no "holes" in $\pi_0(\square E_{0-\infty}B_{0\nu}A_{0\nu'-\infty})$.

4.5. The Poincaré map π

In the D_0 unit coordinate system, $\pi : \overline{R_0} \rightarrow \overline{V_0^{out}}$ is defined by $\pi := \pi_0^{-1} \circ \hat{\pi}_1$ while in the D_1 unit coordinate system, $\pi : \overline{R_1} \rightarrow \overline{V_1^{in}}$ is defined by $\pi := \hat{\pi}_0^{-1} \circ \pi_1$. The inverses π_0^{-1} and $\hat{\pi}_0^{-1}$ are required since π_0 is calculated in reverse time. Though we have just defined two functions with two different domains, they are just different representations of the same Poincaré map and there will be no need to give them separate names.

In the previous section, a paradox was presented that will now be explained. The paradox is that the trajectory $\phi_0^t(Q'')$ from Q'' does not leave the D_0 unit until $t = t_3$ when it crosses the boundary at Q; however, $\pi_0^{-1}(Q'') = Q'$, not Q. It appears that π_0^{-1} does not yield the correct result. The paradox is explained by noting that Q' lies on $\overrightarrow{F_0B_0}$ and is a fixed point of $\hat{\pi}_1$ with a return time of zero seconds. Therefore, $\pi_0^{-1} \circ \hat{\pi}_1 \circ \pi_0^{-1}(Q'') = \pi_0^{-1} \circ \hat{\pi}_1(Q') = \pi_0^{-1}(Q') = Q$ with an elapsed time of $(t'' - t') + (0) + (t') = t''$ as expected.

This discussion illustrates why the domains of the half-maps are taken to be closures. Without the closure, $\hat{\pi}_1$ would not be defined on $\overrightarrow{F_0B_0}$. Of course, $\pi_0(Q)$ could be defined to be Q'' instead of Q', but then the interpretation of π_0 as the first return map is lost.

5. Return/Transfer/Escape Boundaries

The purpose of this section is to classify the behavior of all the entry points of the dual double scroll equation. In the double scroll family, entry points either transfer or return. The opposite stability type of the equilibrium point in region D_1 leads to a third possibility in the dual double scroll family: escape.

Kahlert and Chua performed a return/transfer analysis for the double scroll equation where the boundary separating return and transfer points was found using a limiting process on a family of straight lines [4]. The method developed in this section is new and finds the boundary directly using an implicit equation similar to the equations used to define the Poincaré half-maps π_0 and π_1.

Trajectories that are tangent to the boundaries U_{-1} or U_1 play a crucial role in the return/transfer/escape analysis and it is worthwhile to spend some time discussing them. Consider a two-dimensional PWL system with two parallel boundaries U_1 and U_{-1} that divide the plane into three regions D_{-1}, D_0 and D_1. In Fig. 9(a), the trajectory from the D_0 entry point $\hat{x}$ is tangent to U_{-1} and then goes on to cross U_1. Clearly $\hat{x}$ separates entry points that return from those that transfer. A different case is presented in Fig. 9(b) where the trajectory from $\hat{x}$ is again tangent to U_{-1}, but since the trajectory intersects U_{-1} a second time, entry points on either side of $\hat{x}$ transfer and $\hat{x}$ does not separate different types of entry points. We call such a tangency a *degenerate tangency*.

Though the fact will not be used in this paper, it is interesting to note that, as Fig. 9 illustrates, if $\phi_i^t(\hat{x})$, $(i = 0, 1)$, is tangent to a boundary and $\pi_i(\hat{x}) \neq \hat{x}$, then π_i is discontinuous at $\hat{x}$. Thus π_0 is discontinuous on $\pi_0^{-1}(\overrightarrow{F_0E_0})$ and π_1 is discontinuous on $\pi_1^{-1}(\overrightarrow{F_1B_1})$.

5.1. Return/escape boundary for the D_1 unit

Trajectories entering the D_1 unit will either return to the D_0 unit by crossing V_1 or remain in the D_1 unit as $t \to \infty$. In this section, all D_1 entry points will be specified by their x-y coordinates. We study three cases.

Case 1: $x < 1$. All entry points return. This result is clear since as $t \to \infty$, all trajectories tend along the unstable eigenvector (the positive z-axis) and pass through V_1. A trajectory may be tangent to V_1 at some point of $\overline{F_1B_1}$, but such a trajectory possesses a degenerate tangency.

Case 2: $x = 1$. Consider the eigenplane in the D_1 unit (Fig. 10). Since $\sigma_1 < 0$, the trajectory emanating from B_1 always spirals toward the origin.[3] In reverse time, the trajectory through

[3] Remember that the vector field at B_1 is tangent to the line $x = 1$.

B_1 spirals outward and hits the line $x = 1$ at some point B_1^*. All entry points on $x = 1$ with y-coordinate greater than B_1^* return. Entry points with $B_1 \le y \le B_1^*$ spiral toward the origin and forever remain in the D_1 unit. In the latter case, π_1 is defined to be D_1 and (x, y) is considered to be a return point, not an escape point.

Case 3: $x > 1$. Case 3 is similar to case 2 except that there are now z dynamics that push trajectories away from V_1. Thus, it is expected that most entry points will escape.

In analogy with case 2, if x is fixed at some value x_0, then there exists a y_0 such that the trajectory emanating from (x_0, y_0) is tangent to the boundary plane V_1. The entry points along the line $x = x_0$ with y-coordinate less than y_0 escape while points with $y > y_0$ return. As x_0 is increased from 1, the points (x_0, y_0) trace out a curve Γ_1 which is the boundary between escape and return points for case 3.

To calculate Γ_1, one needs to find all points (x, y) such that the trajectory from (x, y) is tangent to V_1 at its first return. Since the points of tangency must lie on the same side of the eigenplane as (x, y), the only possible points of tangency lie on $\overrightarrow{B_1B_{1\infty}}$. Thus, one can find Γ_1 by calculating the set of first return points of $\overrightarrow{B_1B_{1\infty}}$ *in reverse time*. This is equivalent to calculating $\pi_1^{-1}(\overrightarrow{B_1B_{1\infty}})$.

Calculation of Γ_1:

In the nonlinear u-v coordinate system, $\overrightarrow{B_1B_{1\infty}} = \{ (u, v) \mid u = 0, v > 1 \}$. Let $\hat{x} \in \overrightarrow{B_1B_{1\infty}}$ have x-y coordinates (x, y) and u-v coordinates $(0, v)$.

i) Calculate the inverse return-time function (6) for reverse time, (i.e., $v(u, -t)$) with $u = 0$.

ii) Find the first return time

$$\hat{t} := \min\{ t \ge 0 \mid v(0, -t) = v \} \tag{19}$$

for the trajectory emanating from $(0, v)$.

iii) The first-return point is

$$\pi_1^{-1}(\hat{x}) = e^{-\sigma_1 \hat{t}} \begin{bmatrix} \cos\hat{t} & \sin\hat{t} \\ -\sin\hat{t} & \cos\hat{t} \end{bmatrix} \begin{bmatrix} x \\ y \end{bmatrix}. \tag{20}$$

Γ_1 is the set of points $\pi_1^{-1}(\tilde{x}_1(0, \nu))$ for all $\nu > 1$.

A typical Γ_1 is shown in Fig. 11(a) and the corresponding $\nu(0, -t)$ in Fig. 11(b). Here $\alpha = 9$ and $\beta = 15$. The behavior of $\nu(0, -t)$ is much different from that of $\nu(0, t)$. Each value of ν has an infinite number of return times. The set of *first* return times are between t_1 and t_2. The infinity of return times is not surprising since in reverse time, all trajectories are attracted to the $z = 0$ plane and form expanding spirals that intersect V_1 with every rotation. [4]

Values of ν between 0 and 1 correspond to the segment $\overline{F_1B_1}$. $\pi_1^{-1}(\overline{F_1B_1})$ lies in the half-plane $x < 1$ and, as mentioned before, contains points of degenerate tangency.

Negative values of ν correspond to points on the half-line $\overrightarrow{F_1E_1}$. The first-return times for negative ν can be ignored since trajectories tangent to $\overrightarrow{F_1E_1}$ are incident to V_1 from the D_0 side. These negative values of $\nu(0, -t)$ correspond to virtual trajectories caused by the extension of the D_1 dynamics to all of $\mathbb{R}^3$.

5.2. Return/transfer boundaries for the D_0 unit

Trajectories emanating from D_0 entry points will either return to V_0 or transfer across the D_0 unit to V_0^-.[5]

There are two cases:

Case 1: $x \geq 1$. Due to the expanding spiral nature of the flow ($\sigma_0 > 0$), all entry points transfer. Call the initial x-coordinate $x_0 \geq 1$. π seconds later, the x-coordinate will be $-x_0 e^{\sigma_0 \pi} < -1$ implying that the trajectory has hit V_0^-.

Case 2: $x < 1$. This case is more complicated since there exist both return and transfer points. To illustrate this point, consider an entry point $\hat{x} := (\varepsilon, \varepsilon)$ that is close to C_0. Let $\hat{\phi}$ be the trajectory emanating from $\hat{x}$. For ε small, the z dynamics (governed by $(1 - \varepsilon)e^{\gamma_0 t}$) will die out before the x-y dynamics (governed by $\varepsilon e^{\sigma_0 t}$) have grown to a significant size. Thus, for ε small, the z dynamics can be ignored. Fig. 12 shows a typical $\hat{\phi}$ projected onto the $z = 0$ eigenplane.

[4] Remember that the D_1 dynamics have been extended to all of $\mathbb{R}^3$ when calculating $\nu(0, -t)$.

[5] The trajectory from C_0 will tend toward the origin as $t \to \infty$. It is neither a return nor a transfer point.

Now consider the trajectory $-\hat{\phi}$ that emanates from $-\hat{x}$, also shown in Fig. 12. Ignoring the z dynamics, this trajectory is 180° out of phase with respect to $\hat{\phi}$; hence, if $\hat{\phi}$ returns (transfers), then $-\hat{\phi}$ transfers (returns).

The boundary Γ_0 between return and transfer points consists of points $\hat{x}$ such that $\phi_0^l(\hat{x})$ is tangent to a boundary at its first return. The only possible points of tangency lie on $\overrightarrow{F_0E_0}$ so $\Gamma_0 \subset \pi_0(\overrightarrow{F_0E_0})$. $\pi_0(\overrightarrow{F_0E_0})$ is shown in Fig. 13(a) for $\alpha = 9$ and $\beta = 15$. By shading in the return region (Fig. 13(b)), it is evident that the portion of $\pi_0(\overrightarrow{F_0E_0})$ connecting F_0 and Q'' does not separate return and transfer points and is not, therefore, part of Γ_0; the rest of $\pi_0(\overrightarrow{F_0E_0})$ is Γ_0. Trajectories emanating (in forward time) from $Q''F_0$ have degenerate tangencies.

It is informative to spend more time considering the point Q''. $Q' \in \pi_0(\overrightarrow{E_0E_{0-}})$ so there is some $Q \in \overrightarrow{E_0E_{0-}}$ such that $\pi_0(Q) = Q'$. Furthermore, $Q' \in \overline{F_0E_0}$ which implies that the trajectory $\phi_0^l(Q)$ from point Q is tangent to the boundary at point Q', but does not leave the D_0 unit until it hits points Q''. This situation is precisely the one explained in Section 4.5. Hence, $\pi_0(Q') = Q''$ and $\Gamma_0 = \pi_0(\overrightarrow{Q'E_0})$.

6. Homoclinic and Heteroclinic Orbits

The Poincaré half-maps are extremely useful tools for locating homoclinic and heteroclinic orbits. The conditions for existence of such orbits—to be presented below—are easy to verify visually. Each orbit presented in this section was located in less than five minutes using a program that draws the π_0 and π_1 maps (the same program that generated the figures in this paper). The α-β parameters were adjusted by hand until the existence conditions were satisfied. No optimization routines were required.

The importance of homoclinic orbits is due to

Shilnikov's Theorem: [5]

Let $\xi: \mathbb{R}^3 \to \mathbb{R}^3$ be a continuous piecewise-linear vector field with an equilibrium point $\hat{x}$ with complex conjugate eigenvalues $\sigma \pm j\omega$ with $\omega \neq 0$ and a real eigenvalue γ. If $|\sigma| < |\gamma|$ and there exists a homoclinic orbit at $\hat{x}$, then ξ can be infinitesimally perturbed to a vector field ξ'

such that ξ' possesses a countable number of horseshoes.

Owing to the odd symmetry of (1), P_1 can be identified with P_{-1}. Thus, a heteroclinic orbit from P_1 to P_{-1} can be considered as a homoclinic orbit of P_1 and, if it satisfies the Shilnikov eigenvalue constraints, also implies the existence of a countable number of horseshoes.

Horseshoes [5] yield very complicated trajectories and are an indication that chaotic behavior exists. Shilnikov's theorem is one of the few methods available to show rigorously the existence of horseshoes.

In this section, we demonstrate the existence of two homoclinic orbits—one at P_0 and one at P_1—and one heteroclinic orbit. All three orbits satisfy the Shilnikov eigenvalue constraints and, therefore, indicate that horseshoes exist in the dual double scroll equation. Furthermore, we explain how it occurs that when the homo/heteroclinic orbits exist, there is no observable steady-state behavior (i.e., for almost all initial conditions, the steady state is unbounded). This is an interesting point because it implies that when there is chaos, there is no homo/heteroclinic orbit.

6.1. Homoclinic orbits at the origin

A homoclinic orbit at the origin spirals out from the origin on the D_0 eigenplane, enters region D_1, returns to region D_0 at point C, and then approaches the origin along the stable eigenvector. By symmetry, if a homoclinic orbit exists at the origin, then another one—the reflection of the first through the origin—exists as well.

Conditions for the existence of a homoclinic orbit at the origin:

There exists a homoclinic orbit at the origin iff there exists a point $Q \in \overline{E_0A_0}$ such that (in the D_0 unit)

i) $\hat{\pi}_1(Q) = 0$ and

ii) $\pi_0(Q) = 0$.

In practice, one plots $\hat{\pi}_1(\overline{E_0A_0})$. If it passes through C_0, then condition i) is satisfied. Let (u', v') be the u-v coordinates of Q. Since $Q \in \overline{E_0A_0}$, $u' = 1$ and $0 < v' < 1$. Next, plot

$\pi_0(\overline{B_{0\nu'}A_{0\nu'}})$ where $\overline{B_{0\nu'}A_{0\nu'}} := \{(u, v) \mid 0 \le u \le 1, v = \nu'\}$. If it wraps around C_0, then condition ii) is satisfied.

Fig. 14 shows $\hat{\pi}_1(\overline{E_0A_0})$ for $\alpha = 160$ with $\beta = 240$ (Fig. 14(a)), and $\beta = 280$ (Fig. 14(b)). Clearly for some $240 < \beta < 280$, $\hat{\pi}_1(\overline{E_0A_0})$ must pass through C_0. Fig. 14(c) is $\hat{\pi}_1(\overline{E_0A_0})$ for $\beta = 260$ showing that condition i) is satisfied for some β near 260. Fig. 14(d) shows $\pi_0(\overline{B_0A_0})$ for $\alpha = 160$ and $\beta = 260$. $\overline{B_0A_0}$ corresponds to $v = 1$ and since $\pi_0(\overline{B_0A_0})$ wraps around the origin, $\pi_0(\overline{B_{0\nu'}A_{0\nu'}})$ must also wrap around the origin for $0 < \nu' < 1$. Hence, condition ii) is satisfied and a homoclinic orbit exists at the origin.

The eigenvalues for these parameters are $\tilde{\sigma}_0 = 1.00$, $\tilde{\omega}_0 = 15.6$ and $\tilde{\gamma}_0 = -48.7$. Shilnikov's theorem is satisfied and a countable number of horseshoes exist.

Of course, one can never observe the homoclinic orbit directly using computer simulations; however, it is sometimes possible to observe a trajectory that repeatedly passes near the homoclinic orbit. Such trajectories can be observed for a heteroclinic orbit of the double scroll [6]; the hole-filling trajectories of the double scroll presented in [1] are another example. If such a trajectory exists, we call the homoclinic orbit *observable*.

Unfortunately, this homoclinic orbit is not observable; all computer simulations with this set of parameters become unbounded. The reason is evident from Fig. 14(d) which shows $\pi_0(\overline{B_0A_0})$ and $\pi_0(\overline{B_{0\nu'}A_{0\nu'}})$ for $\nu' = 1.2$. Both spirals wrap around C_0 implying that the quadrilateral $\square A_0B_0B_{0\nu'}A_{0\nu'}$ maps into a snake that spirals around C_0. Thus every neighborhood of the origin contains points of $\pi_0(\square A_0B_0B_{0\nu'}A_{0\nu'})$. Equivalently, every neighborhood of the origin contains points that π_0^{-1} maps below $\overline{B_0A_0}$. A calculation of the return/escape boundary for π_1 indicates that points below $\overline{B_0A_0}$ are escape points for $\hat{\pi}_1$. Hence, *every neighborhood of the homoclinic orbit at the origin contains trajectories that are unbounded*.

Different values of α and β can also yield homoclinic orbits at the origin. In fact, there is a curve in the α-β plane consisting of parameter values for which there are homoclinic orbits at the origin. All of these homoclinic orbits have been found to be unobservable as well.

To illustrate a case where one of the conditions is not met, Fig. 15 shows $\hat{\pi}_1(\overline{E_0A_0})$ and $\pi_0(\overline{B_{0\nu'}A_{0\nu'}})$ for $\alpha = 20$ and $\beta = 40$. Condition i) is satisfied, but ii) is not. For this case, $\nu' \approx 0.99$ and, as Fig. 15 shows, $\pi_0(\overline{B_{0\nu'}A_{0\nu'}})$ does not wind around C_0. In fact, $\pi_0(\overline{B_{0\nu'}A_{0\nu'}})$ does not wrap around C_0 for any $\nu' > 0.55$.

6.2. Homoclinic orbits at P_1

A homoclinic orbit at P_1 leaves P_1 along the real eigenvector, enters region D_0 at D, returns to region D_1 somewhere on $\overleftrightarrow{AB}$ and then spirals in to P_1 on the D_1 eigenplane. By symmetry, if a homoclinic orbit exists at P_1, then another one—the reflection of the first through the origin—exists at P_{-1} as well.

Conditions for the existence of a homoclinic orbit at P_1:

There exists a homoclinic orbit at P_1 iff there exists a point $Q \in \overline{B_1A_1}$ such that (in the D_1 unit)

i) $\hat{\pi}_0(Q) = D_1$ and

ii) $\pi_1(Q) = D_1$.

In practice, one plots $\hat{\pi}_0(\overline{B_1A_1})$. If it passes through D_1, then condition i) is satisfied. Let (u', ν') be the u-ν coordinates of Q. Since $Q \in \overline{B_1A_1}$, $0 < u' < 1$ and $\nu' = 1$. Next, plot $\pi_1(\overline{E_{1u'}A_{1u'}})$ where $\overline{E_{1u'}A_{1u'}} := \{(u, \nu) \mid u = u', 0 \le \nu \le 1\}$. If it wraps around D_1, then condition ii) is satisfied.

Fig. 16(a) shows $\hat{\pi}_0(\overline{B_1A_1})$ and $\pi_1(\overline{E_1A_1})$ for $\alpha = 50$ and $\beta = 65$. Condition i) is satisfied since $D_1 \in \hat{\pi}_0(\overline{B_1A_1})$. Condition ii) is satisfied as well: the fact that $\pi_1(\overline{E_1A_1})$ spirals around D_1 implies that $\pi_1(\overline{E_{1u'}A_{1u'}})$ wraps around D_1 for any $0 \le u' \le 1$.

The eigenvalues for these parameters are $\tilde{\sigma}_0 = -1.93$, $\tilde{\omega}_0 = 6.56$ and $\tilde{\gamma}_0 = 10.0$. Shilnikov's theorem is satisfied and a countable number of horseshoes exist.

However, once again the homoclinic orbit is not observable in computer simulations. Fig. 16(b) shows $\hat{\pi}_0(\overline{B_1A_1})$ and $\hat{\pi}_0(\overline{B_{1\nu}A_{1\nu}})$ for $\nu = 1.2$. Every neighborhood of D_1 contains points in

$\hat{\pi}_0(\square A_1B_1B_{1v}A_{1v})$. In other words, every neighborhood of D_1 contains points that $\hat{\pi}_0^{-1}$ maps to the right of $\overline{B_1A_1}$ which is located in the escape region for π_1. Hence, *every neighborhood of the homoclinic orbit at* P_1 *contains trajectories that are unbounded*.

Just as for homoclinic orbits at the origin, there exists an entire family of homoclinic orbits at P_1. All of these orbits have been found to be unobservable.

6.3. Heteroclinic orbits

A heteroclinic orbit leaves P_{-1} along the real eigenvector, enters region D_0 at $-D$, crosses region D_0, enters region D_1 somewhere on $\overleftrightarrow{AB}$ and then spirals in to P_1 on the D_1 eigenplane. By symmetry, if a heteroclinic orbit exists, then another one—the reflection of the first through the origin—exists as well.

Conditions for the existence of a heteroclinic orbit:

There exists a heteroclinic orbit iff there exists a point $Q \in \overrightarrow{A_1A_{1\infty}}$ such that (in the D_1 unit)

i) $\hat{\pi}_0(Q) = D_1$ and

ii) $\pi_1(Q) = D_1$.

In practice, one plots $\hat{\pi}_0(\overrightarrow{A_1A_{1\infty}})$. If it passes through D_1, then condition i) is satisfied. Let (u', v') be the u-v coordinates of Q. Since $Q \in \overrightarrow{A_1A_{1\infty}}$, $u' > 1$ and $v' = 1$. Next, plot $\pi_1(\overline{E_{1u'}A_{1u'}})$. If it wraps around D_1, then condition ii) is satisfied.

Fig. 17 shows $\hat{\pi}_0(\overrightarrow{A_1A_{1\infty}})$ and $\pi_1(\overline{E_{1u'}A_{1u'}})$ where $u' = 1.12$ and the parameters are $\alpha = 25$ and $\beta = 26.7$.

The eigenvalues for these parameters are $\tilde{\sigma}_0 = -1.60$, $\tilde{\omega}_0 = 3.74$ and $\tilde{\gamma}_0 = 5.77$. Shilnikov's theorem is satisfied and a countable number of horseshoes exist.

However, this heteroclinic orbit is unobservable for the same reason as the two homoclinic orbits. Namely, every neighborhood of D_1 contains points that $\hat{\pi}_0^{-1}$ maps into the escape region of π_1. Hence, *every neighborhood of the heteroclinic orbit contains trajectories that are*

unbounded. Furthermore, the entire family of heteroclinic orbits has been found to be unobservable.

7. Bifurcation Analysis

In this section, the region in the α-β plane where a stable attracting set exists is located as well as the locus of points where the Hopf bifurcation occurs. First, the parameter values for which (1) belongs to the dual double scroll family is identified.

7.1. The dual double scroll boundary

The dual double scroll equation (1) belongs to the dual double scroll family whenever each equilibrium point possesses a complex conjugate pair of eigenvalues and when $\bar{\gamma}_0 < 0$ and $\bar{\gamma}_1 > 0$. In region D_i, $(i = 0, 1)$, the characteristic polynomial of (1) is

$$s^3 + (\alpha m_i + 1)s^2 + \alpha(m_i - \alpha + \beta)s + \alpha\beta m_i. \tag{21}$$

The closed-form equations for the zeros of a third-order polynomial are well known. Let

$$a_i := (\alpha m_i - \alpha + \beta)/3 - (\alpha m_i + 1)^2/9 \tag{22}$$

and

$$b_i := (\alpha m_i + 1)^3/27 - (\alpha m_i + 1)(\alpha m_i - \alpha + \beta)/6 + \alpha\beta m_i/2. \tag{23}$$

There exists complex zeros of (21) iff $a_i^3 + b_i^2 > 0$. The locus S defined by $a_1^3 + b_1^2 = 0$ is shown in Fig. 18. The locus $a_0^3 + b_0^2 = 0$ lies below S so is of no consequence. Thus, for all (α, β) above S in Fig. 18, (1) possesses complex eigenvalues in each region. For (α, β) below S, there are three real eigenvalues in region D_1.

It remains to determine the signs of $\bar{\gamma}_0$ and $\bar{\gamma}_1$. In terms of the eigenvalues, the characteristic polynomial can be written as

$$(s - \bar{\gamma}_i)((s - \bar{\sigma}_i)^2 + \bar{\omega}_i^2) \tag{24}$$

which expands to

$$s^3 - (\bar{\gamma}_i + 2\bar{\sigma}_i)s^2 + (\bar{\sigma}_i^2 + \bar{\omega}_i^2 - 2\bar{\sigma}_i\bar{\gamma}_i)s - \bar{\gamma}_i(\bar{\sigma}_i^2 + \bar{\omega}_i^2). \tag{25}$$

Comparing the last term of (21) with that of (25), it is evident that for $\alpha, \beta > 0$, the sign of m_i is opposite that of $\bar{\gamma}_i$. Therefore, $m_0 = 2/7$ implies $\bar{\gamma}_0 < 0$ and $m_1 = -1/7$ implies $\bar{\gamma}_1 > 0$.

Thus, for all (α, β) above S in Fig. 18, (1) belongs to the dual double scroll family. It is this region where the analysis presented in this paper applies.

7.2. The Hopf bifurcation

A Hopf bifurcation[6] occurs when the pair of complex conjugate eigenvalues at the origin $(\bar{\sigma}_0 \pm j\bar{\omega}_0)$ lie on the imaginary axis, that is when $\bar{\sigma}_0 = 0$. The characteristic polynomial (24) becomes

$$s^3 + \bar{\gamma}_0 s^2 + \bar{\omega}_0^2 s + \bar{\gamma}_0 \bar{\omega}_0^2 \tag{26}$$

for $\bar{\sigma}_0 = 0$. Comparing coefficients of (21) and (26), $\bar{\sigma}_0 = 0$ implies

$$(\alpha m_0 + 1)(\alpha m_0 - \alpha + \beta) = \alpha\beta m_0 \tag{27}$$

which can be rewritten as

$$\beta = (m_0 - m_0^2)\alpha^2 + (1 - m_0)\alpha \;=:\; H(\alpha). \tag{28}$$

For $\beta > H(\alpha)$, the origin is a stable equilibrium point. For β just less than $H(\alpha)$, computer simulations show that there exists a stable limit cycle just as the Hopf theorem would predict. $H(\alpha)$ is plotted in Fig. 18.

It is interesting to note that as the magnification in Fig. 18(b) shows, the curves S and H intersect near $(\alpha, \beta) = (1.2, 1.2)$. Remember that (1) belongs to the dual double scroll family only for parameter values above S.

7.3. Trapping Regions

A *trapping region* T is some bounded, open set such that $\pi(T) \subset T$. Since $\pi = \pi_0^{-1} \circ \hat{\pi}_1$, an equivalent statement is that $\hat{\pi}_1(T) \subset \pi_0(T)$. Any orbit of the Poincaré map with initial condition in T will forever remain in T. Thus T must contain a stable (and observable) attracting set.

For the homoclinic and heteroclinic orbits discussed in Section 5, π_0^{-1} mapped some points in any neighborhood of the orbit into the escape region of π_1. Thus, no trapping region exists for any of these orbits.

---

[6] The Hopf bifurcation theorem has not been proved for PWL ODEs; the term is used here because the bifurcation possesses the essential features of a Hopf bifurcation.

Fig. 19 shows a case where a trapping region does exist. There are two regions shown in Fig. 19: $\pi_0(T_{u'})$ and $\hat{\pi}_1(T_{u'})$ where the trapping region is

$$T_{u'} := \{(u, v) \mid 0 < u < u', 0 < v < 1\}. \tag{29}$$

The constraint $v < 1$ guarantees that no point in $T_{u'}$ is an escape point of $\hat{\pi}_1$. This example is for $\alpha = 9$, $\beta = 15$ and $u' = 1.5$,

In Fig. 20, β is decreased to 12.7. For $u' = 1.2$ (Fig. 20(a)), $\hat{\pi}_1(T_{u'})$ just touches $Q'A'_{0u'}$ but crosses outside of $\pi(T_{u'})$ near $E'_{0u'}A'_{0u'}$. In Fig. 20, $A'_{0u'} := \pi_0(A_{0u'})$ and $E'_{0u'} := \pi_0(E_{0u'})$. For $u' = 1.28$ (Fig. 20(b)), it is precisely the opposite situation: $\hat{\pi}_1(T_{u'})$ just touches $E'_{0u'}A'_{0u'}$, but lies outside of $\pi_0(T_{u'})$ near $Q'A'_{0u'}$. It follows that no trapping region $T_{u'}$ exists. The fact that one cannot find a trapping region of the form $T_{u'}$ does not by itself imply that no trapping region exists; however, computer simulations of (1) show that when no trapping region $T_{u'}$ can be found, all simulations are unbounded.

For a given α, there exists a $\beta(\alpha)$ such that $\beta > \beta(\alpha)$ implies that a trapping region $T_{u'}$ exists and for $\beta < \beta(\alpha)$, there is no trapping region $T_{u'}$. At $\beta = \beta(\alpha)$, there exists a u' such that both $Q'A'_{0u'}$ and $E'_{0u'}A'_{0u'}$ are tangent to the boundary of $\hat{\pi}_1(T_{u'})$. In Fig. 18, the locus of points $\beta(\alpha)$ is plotted on the α-β plane as curve T. For (α, β) above T and below H, a trapping $T_{u'}$ exists implying the existence of a stable attracting set. For (α, β) below T, no trapping $T_{u'}$ exists and computer simulations lead us to believe that there are no stable attracting sets.

8. Existence of a Period One Limit Cycle

As a final demonstration of the analytical power of the Poincaré half-maps, we use them to show the existence of a period one limit cycle.

The idea is illustrated in Fig. 21 for $\alpha = 9$ and $\beta = 20$: Pick $u' > 1$, such that $\pi_0(\overline{E_{0u}A_{0u}})$ intersects $\hat{\pi}_1(\overline{E_{0u}A_{0u}})$ for $u = u'$ but not for any $u > u'$. Call the point of intersection Q. As u is decreased from u', the point of intersection Q traces out a curve $Q(u)$. Let $\pi_0^{-1}(Q(u))$ have u-v coordinates $(u, v_0(u))$ and let $\hat{\pi}_1^{-1}(Q(u))$ have coordinates $(u, v_1(u))$. For Fig. 21, $u' = 1.8$, $v_0(u') = 0.0$ and $v_1(u') = 0.81$. Fig. 21 also shows $\pi_0(\overline{E_{0u''}A_{0u''}})$ and $\hat{\pi}_1(\overline{E_{0u''}A_{0u''}})$ for $u'' = 1.01$.

Here, $v_0(u'') = 0.29$ and $v_1(u'') = 0.24$. Since $v_0(u') < v_1(u')$, $v_0(u'') > v_1(u'')$ and both v_0 and v_1 are continuous, there is some $\hat{u}$, $u'' < \hat{u} < u'$, such that $v_0(\hat{u}) = v_1(\hat{u}) =: \hat{v}$. The point $(\hat{u},\hat{v})$ is a fixed point of π and corresponds to a period one limit cycle of (1).

Note that for these values of α and β, a trapping region $T_{u'}$ exists for $u = 2.0$. $\hat{u} < 2.0$ so the limit cycle lies within the trapping region though this fact does not imply that the limit cycle is stable. We know of no simple way of determining stability by looking at plots of π_0 and π_1. Computer simulations show that the fixed point found above corresponds to the stable period one solution mentioned in Section 2.

As β is decreased, this period one limit cycle bifurcates to a stable period two limit cycle at $\beta \approx 13.9$; however, a fixed point analysis of π for $\beta = 13$. shows a period one limit cycle still exists. This dilemma can be resolved by realizing that period-doubling theory predicts that after bifurcation, the period one limit cycle still exists but is unstable. Computer simulations show that the period one limit cycle $\beta = 13$ does exist and is, indeed, unstable.

9. Acknowledgements

The authors would like to thank Peter Kennedy and Mireille Broucke for their helpful comments on the manuscript. T. Parker gratefully acknowledges the John and Fannie Hertz Foundation for its support.

References

1. L.O. Chua, M. Komuro, and T. Matsumoto, "The Double Scroll Family Part I and Part II," *IEEE Trans. Circuit Syst.*, November 1986.

2. T. Matsumoto, L.O. Chua, and M. Komuro, "The Double Scroll," *IEEE Trans. Circuit Syst.*, vol. CAS-32, pp. 797-818, August 1985.

3. C.T. Sparrow, "Chaos in a Three-Dimensional Single Loop Feedback System with a Piecewise-Linear Feedback Function," *J. Math. Anal. Appl.*, vol. 83, no. 6, pp. 275-291, 1981.

4. C. Kahlert and L.O. Chua, "Transfer Maps and Return Maps for Piecewise-Linear Three-Region Dynaamical Systems," *Int. Jour. Circ. Theory Appl.*, 1986 (in press).

5. J. Guckenheimer and P. Holmes, *Nonlinear Oscillations, Dynamical Systems and Bifurcations of Vector Fields*, Springer Verlag, New York, 1983.

6. A.I. Mees and P.B. Chapman, "Homoclinic and Heteroclinic Orbits in the Double Scroll Family," *IEEE Trans. Circuit Syst.*, in press.

Figure Captions

Fig. 1 Steady state behavior of the dual double scroll equation for $\alpha = 9$ with (a) $\beta = 20$: symmetric period one; (b) $\beta = 14.5$: asymmetric period one; (c) $\beta = 13.8$: asymmetric period two; (d) $\beta = 13.6$: asymmetric chaos; (e) $\beta = 13.5$: symmetric chaos; (f) $\beta = 13.28$: period five.

Fig. 2 The geometry of the original vector field and of the D_0 and D_1 units.

Fig. 3 π_1 for $\alpha = 9$ and $\beta = 15$ corresponding to monotone $v(u, t)$. (a) $\pi_1(\overrightarrow{F_1B_1})$ and $\pi_1(\overrightarrow{E_1A_1})$; (b) the first return map $v(0, t)$.

Fig. 4 π_0 for $\alpha = 9$ and $\beta = 13$ corresponding to monotone u^+ and u^-. (a) $\pi_0(\overrightarrow{F_0E_0})$; (b) $u^+(0, t)$ and $u^-(0, t)$.

Fig. 5 π_0 for $\alpha = 9$ and $\beta = 13$ corresponding to monotone u^+ and non-monotone u^- with no overlapping. (a) $\pi_0(\overrightarrow{B_{0v}A_{0v}})$ for $v = 0.5$; (b) $u^+(0.5, t)$ and $u^-(0.5, t)$.

Fig. 6 Abstracted trajectories of a two-dimensional system demonstrating the different behaviors for non-monotone u^-. (a) $u^-(v, t)$; (b) $u > u_2$; (c) $u = u_2$; (d) $u_1 < u < u_2$; (e) $u = u_1$; (f) $u < u_1$.

Fig. 7 π_0 for $\alpha = 9$ and $\beta = 13$ corresponding to monotone u^+ and non-monotone u^- with overlapping. (a) $\pi(\overrightarrow{B_0A_0})$; (b) $u^+(1.0, t)$ and $u^-(1.0, t)$.

Fig. 8 The wedge $\square E_{0-}B_{0v}A_{0v-}$ is mapped onto $\square A'_{0v-}Q'B_{0v}Q''E'_{0-}$ by π_0. $\pi_0(\overrightarrow{B_{0v}A_{0v}})$ is plotted for several values of v, $0 \le v \le 1.2$.

Fig. 9 Abstracted trajectories of a two-dimensional system showing how an entry point $\hat{x}$ with a trajectory tangent to a boundary will either (a) separate return points from transfer points or (b) just cause a discontinuity in the return map.

Fig. 10 The eigenplane of the D_1 unit with the trajectory that is tangent to V_1 at B_1.

Fig. 11 (a) Return and escape regions of the D_1 unit for $\alpha = 9$ and $\beta = 15$; (b) $v(0, -t)$ for the return/escape boundary Γ_1.

Fig. 12 Projection onto the D_0 eigenplane of two trajectories each with entry point close to C_0. The trajectory $\phi_0^t(\hat{x})$ hits a different boundary than the one from $\phi_0^t(-\hat{x})$. If $\phi_0^t(\hat{x})$ returns (transfers), then $\phi_0^t(-\hat{x})$ transfers (returns).

Fig.13 Return/transfer regions of the D_0 unit for $\alpha = 9$ and $\beta = 15$. (a) $\pi_0(\overrightarrow{F_0E_0})$; (b) Γ_0 and the return and transfer regions.

Fig. 14 Images of π_0 and $\hat{\pi}_1$ showing the existence of a homoclinic orbit at the origin for $\alpha = 160$ and $\beta = 260$. (a) for $\beta = 240$, C_0 lies below $\hat{\pi}_1(\overline{E_0A_0})$; (b) for $\beta = 280$, C_0 lies above $\hat{\pi}_1(\overline{E_0A_0})$; (c) for $\beta = 260$, $\hat{\pi}_1(\overline{E_0A_0})$ contains C_0; (d) $\pi_0(\overline{B_0A_0})$ wraps around C_0 as does $\pi_0(\overline{B_{0\nu}A_{0\nu}})$ for $\nu = 1.2$.

Fig. 15 Images of π_0 and $\hat{\pi}_1$ showing that a homoclinic orbit does not exist at the origin for $\alpha = 20$ and $\beta = 40$. C_0 lies on $\hat{\pi}_1(\overline{E_0A_0})$ and $\pi_0(\overline{B_{0\nu'}A_{0\nu'}})$ does not wrap around C_0.

Fig. 16 Images of $\hat{\pi}_0$ and π_1 showing the existence of a homoclinic orbit at P_1 for $\alpha = 50$ and $\beta = 65$. (a) D_1 lies on $\hat{\pi}_0(\overline{B_1A_1})$ and $\pi_1(\overline{E_1A_1})$ wraps around D_1; (b) $\hat{\pi}_0(\overline{B_1A_1})$ and $\hat{\pi}_0(\overline{B_{1\nu}A_{1\nu}})$ for $\nu = 1.2$.

Fig. 17 Images of $\hat{\pi}_0$ and π_1 showing the existence of a hetéroclinic orbit for $\alpha = 25$ and $\beta = 26.7$. D_1 lies on $\hat{\pi}_0(\overrightarrow{A_1A_{1\infty}})$ and $\pi_1(\overline{E_{1u'}A_{1u'}})$ wraps around D_1.

Fig. 18 Bifurcation diagram. (a) The dual double scroll equation belongs to the dual double scroll (DDS) family for parameters lying above S. Along the curve H, a Hopf bifurcation occurs. For parameters above H, the origin is a stable equilibrium point. T is the trapping region boundary. For parameters lying between H and T, a stable attracting set exists. Below T, no trapping region exists and, therefore, there are no stable attracting sets. (b) a magnification more clearly showing the intersection of S and H.

Fig. 19 For $\alpha = 9$ and $\beta = 15$, $\hat{\pi}_1(T_{u'})$ is contained in $\pi_0(T_{u'})$; therefore, $T_{u'}$ is a trapping region.

Fig. 20 No trapping region exists for $\alpha = 9$ and $\beta = 12.7$. (a) For $u' = 1.2$, $\hat{\pi}_1(T_{u'})$ just lies

within $\pi_0(T_{u'})$ along $Q'A'_{0u'}$, but lies outside near $E'_{0u'}A'_{0u'}$. (a) For $u' = 1.27$, $\hat{\pi}_1(T_{u'})$ just lies within $\pi_0(T_{u'})$ along $E'_{0u'}A'_{0u'}$, but lies outside near $Q'A'_{0u'}$.

Fig. 21 Plots of $\pi_0(\overline{E_{0u}A_{0u}})$ and $\hat{\pi}_1(\overline{E_{0u}A_{0u}})$ demonstrating the existence of a period one limit cycle for $\alpha = 9$ and $\beta = 20$. $\pi_0^{-1}(Q') = (u', v_0(u'))$, $\hat{\pi}_1^{-1}(Q') = (u', v_1(u'))$, $\pi_0^{-1}(Q'') = (u'', v_0(u''))$ and $\hat{\pi}_1^{-1}(Q'') = (u'', v_1(u''))$. Since $v_0(u') < v_1(u')$ and $v_0(u'') > v_1(u'')$, there exists a fixed point of π for some $(\hat{u}, v_0(\hat{u}))$ with $u'' < \hat{u} < u'$.

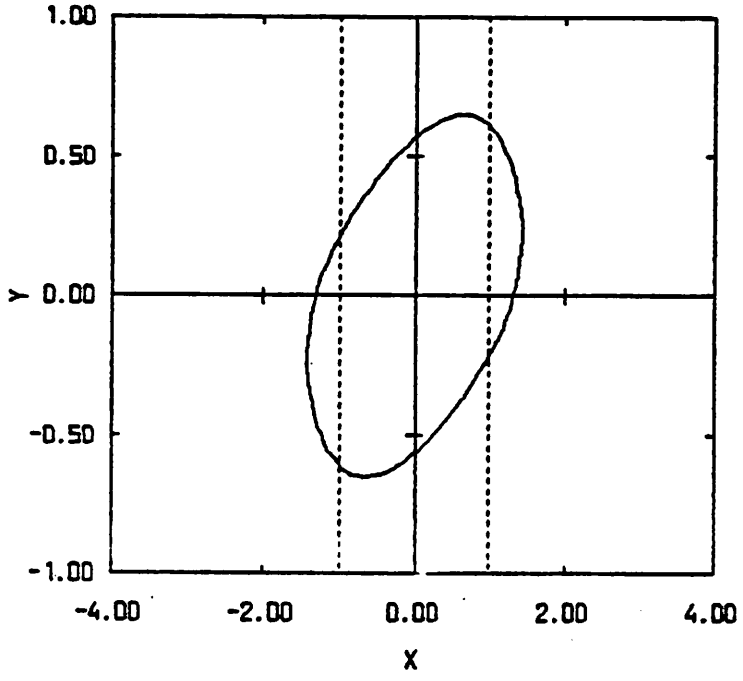

Figure 1(a)

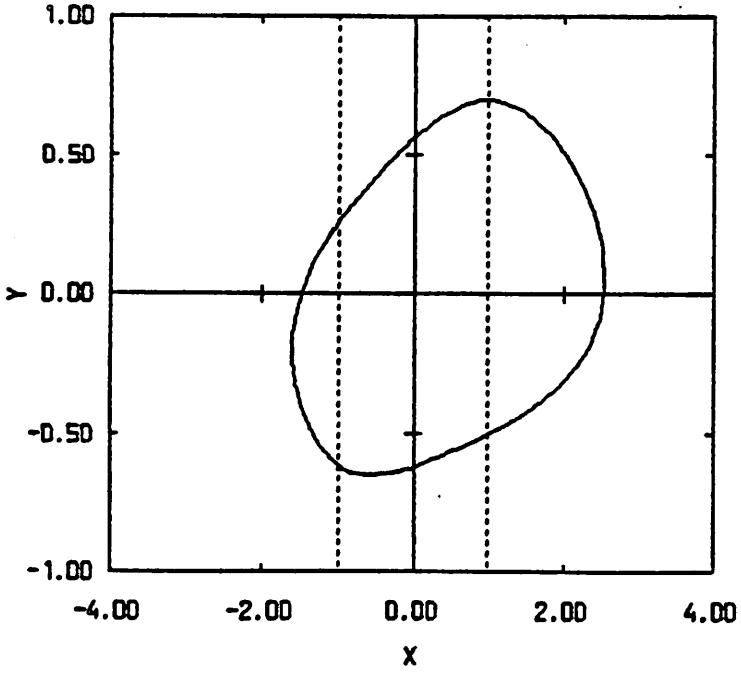

Figure 1(b)

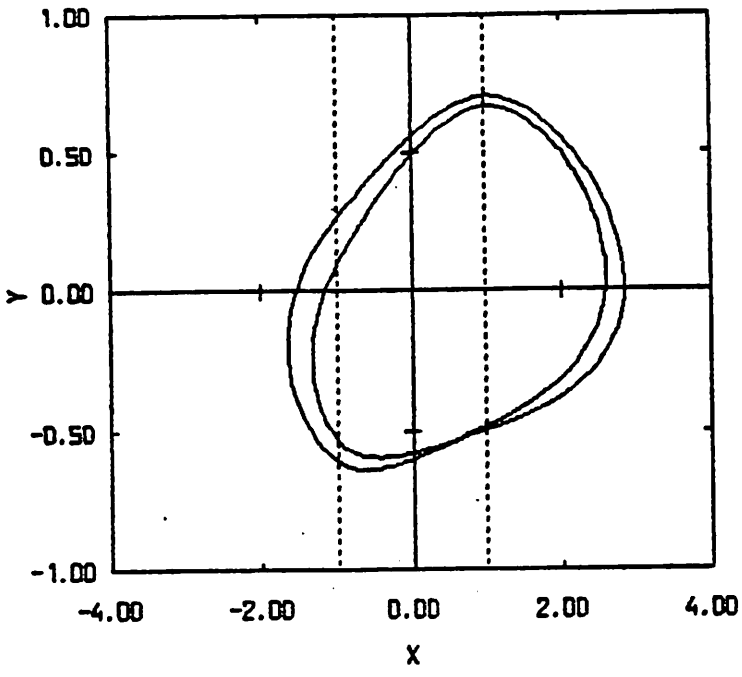

Figure 1(c)

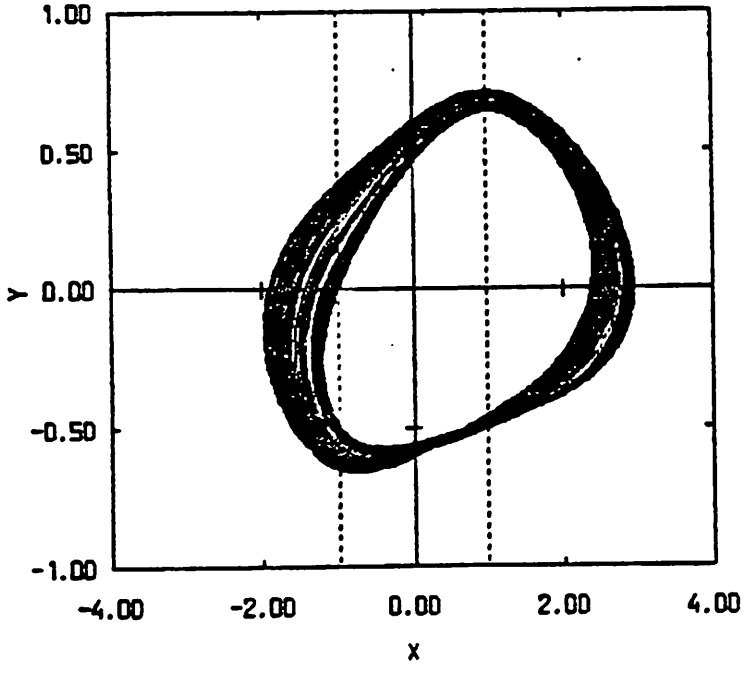

Figure 1(d)

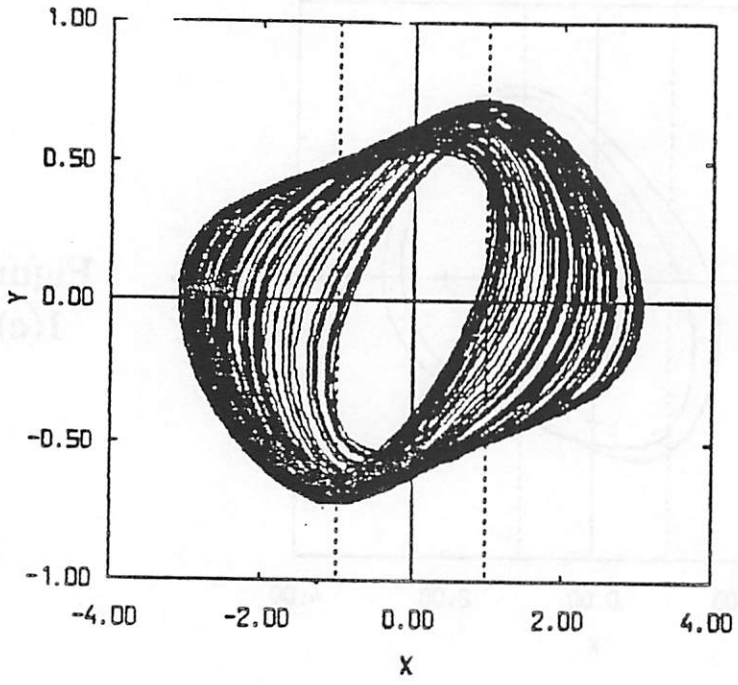

Figure 1(e)

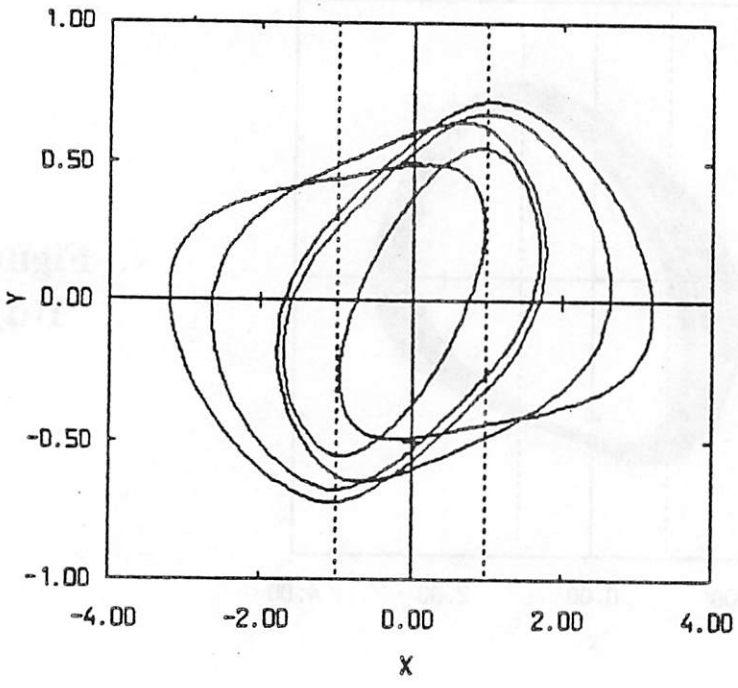

Figure 1(f)

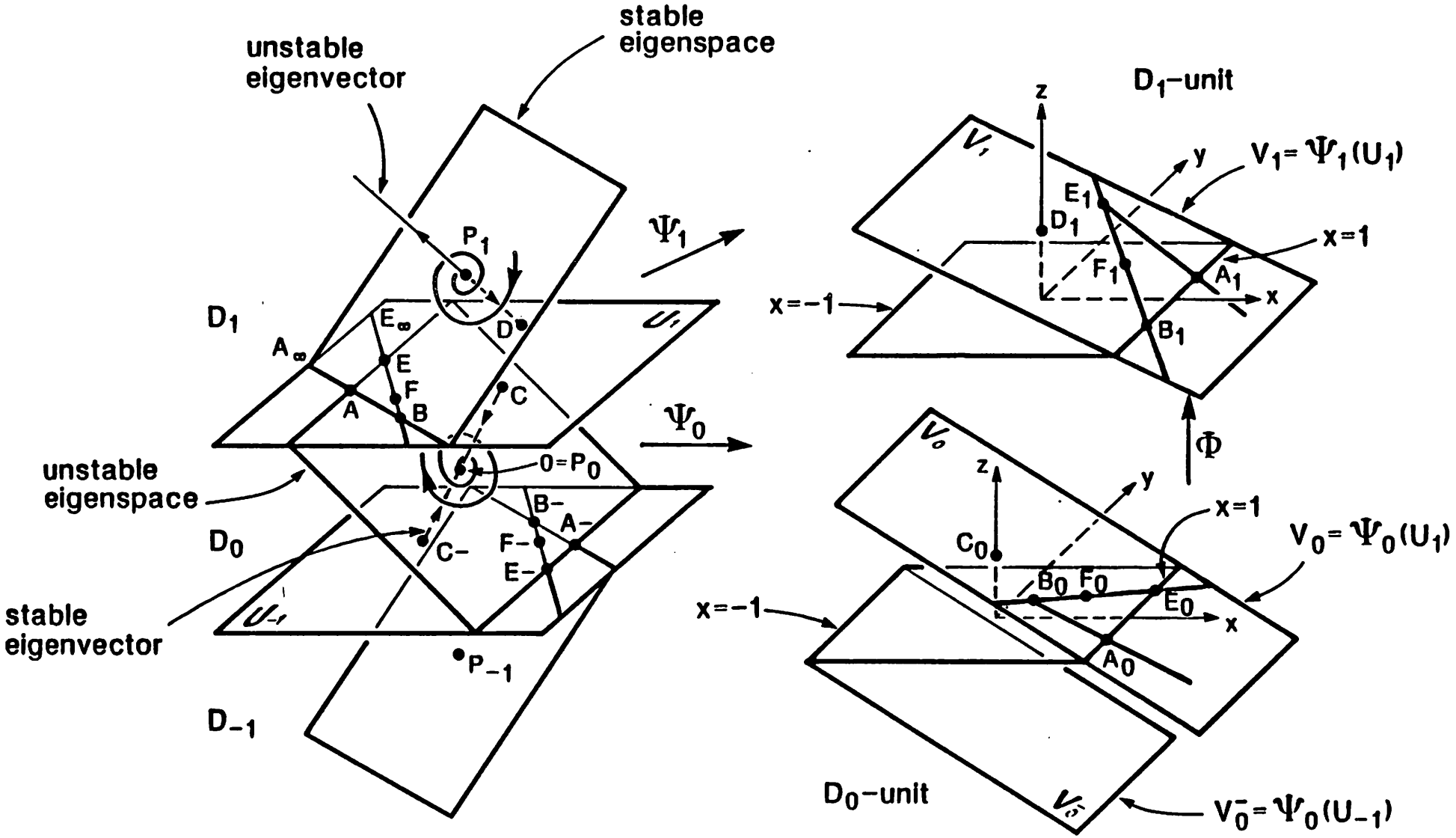
unstable
eigenvector
stable
eigenspace
D_1
P_1
Ψ_1
E_∞
A_∞
E
F
A
B
D
C
U_1
Ψ_0
unstable
eigenspace
D_0
0=P_0
B−
A−
C−
F−
E−
stable
eigenvector
U_{-1}
P_{-1}
D_{-1}
D_1−unit
z
y
V_1= $\Psi_1(U_1)$
E_1
D_1
x=1
F_1
A_1
x
x=−1
B_1
V_1
Φ
V_0
z
y
x=1
C_0
V_0= $\Psi_0(U_1)$
B_0 F_0
E_0
x
x=−1
A_0
D_0−unit
V_{-1}
V_0^-= $\Psi_0(U_{-1})$

Figure 2

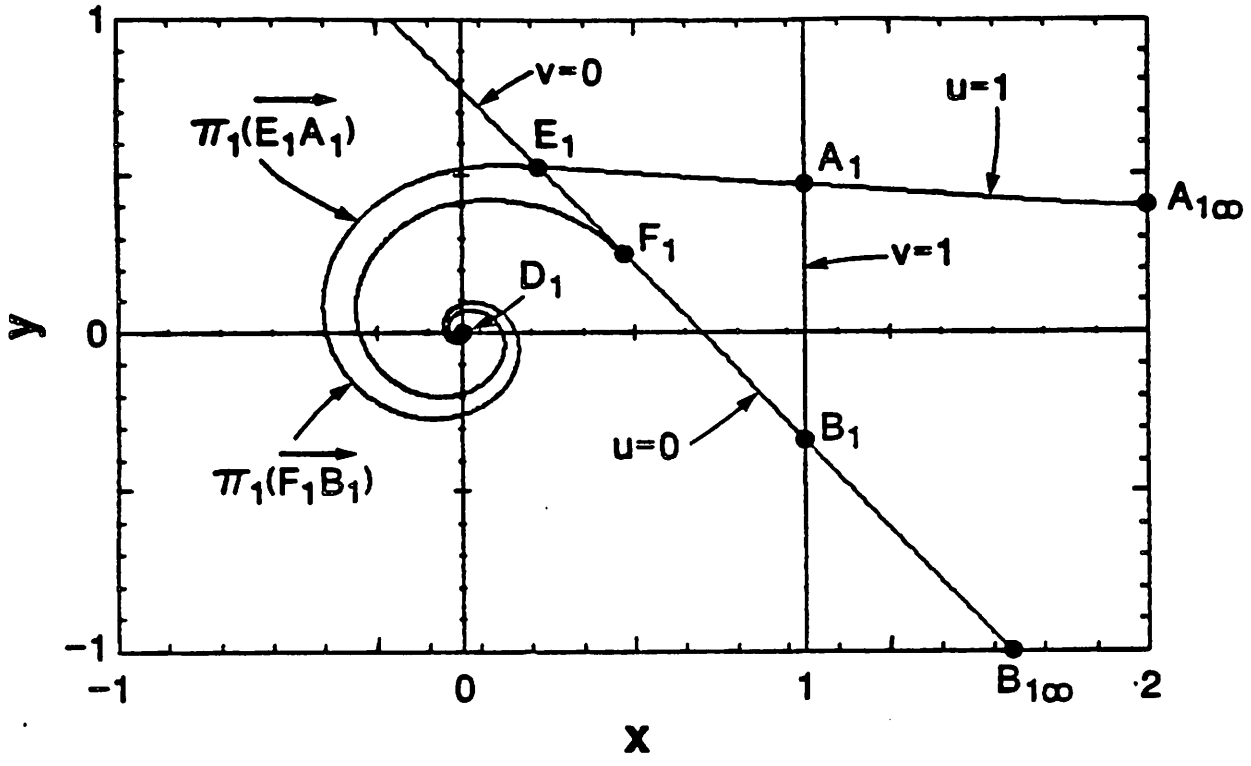
1
0
−1
−1
0
1
2
x
y
v=0
u=1
v=1
u=0
$\overrightarrow{\pi_1(E_1A_1)}$
$\overrightarrow{\pi_1(F_1B_1)}$
E_1
A_1
$A_{1\infty}$
F_1
D_1
B_1
$B_{1\infty}$

Figure 3(a)

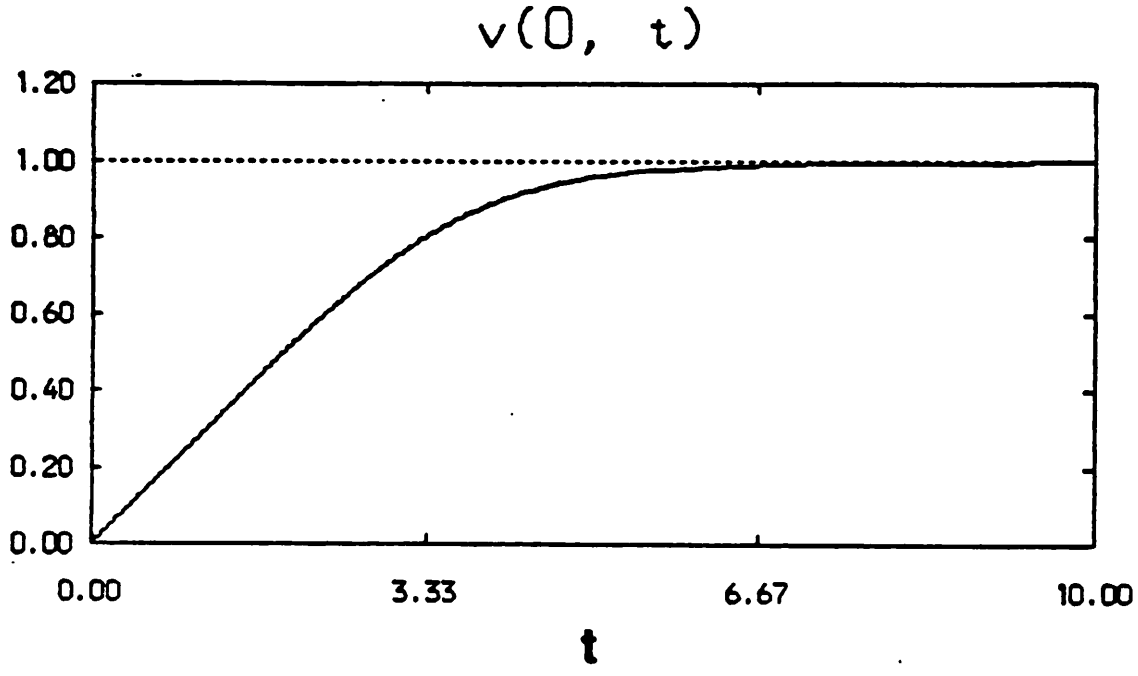

Figure 3(b)

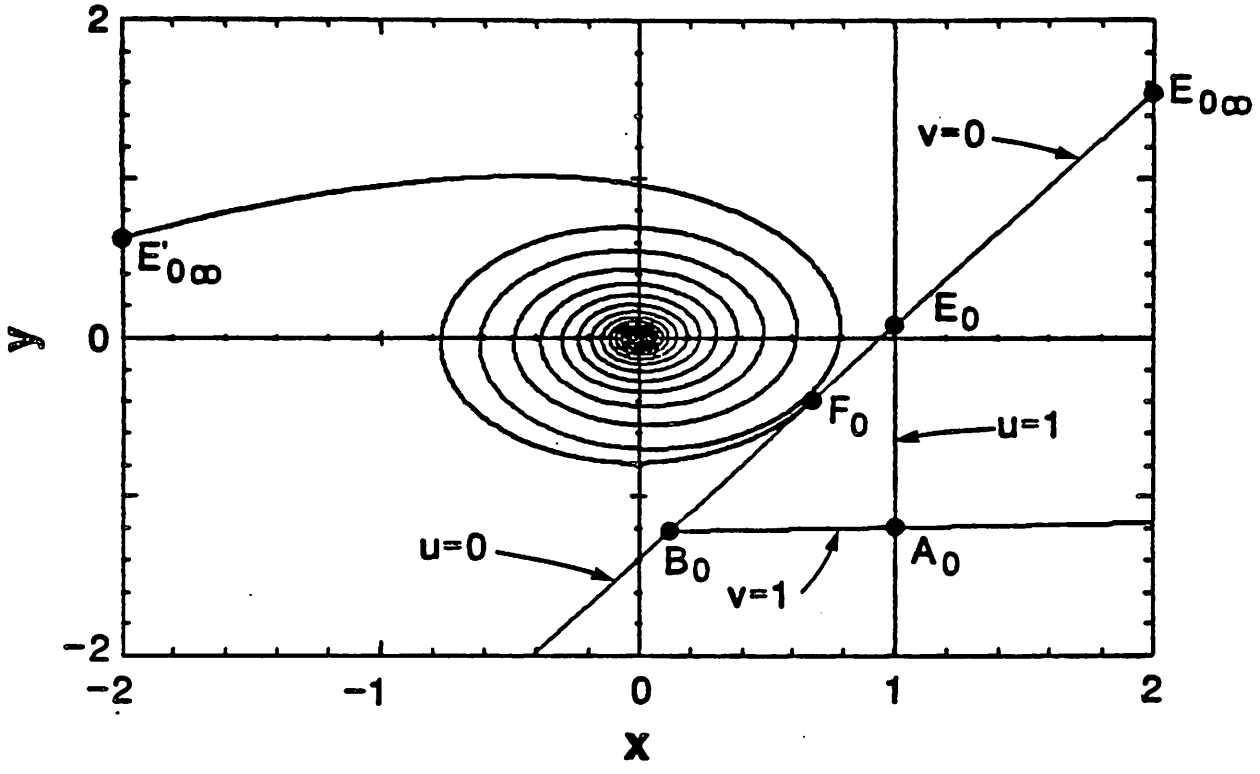

Figure 4(a)

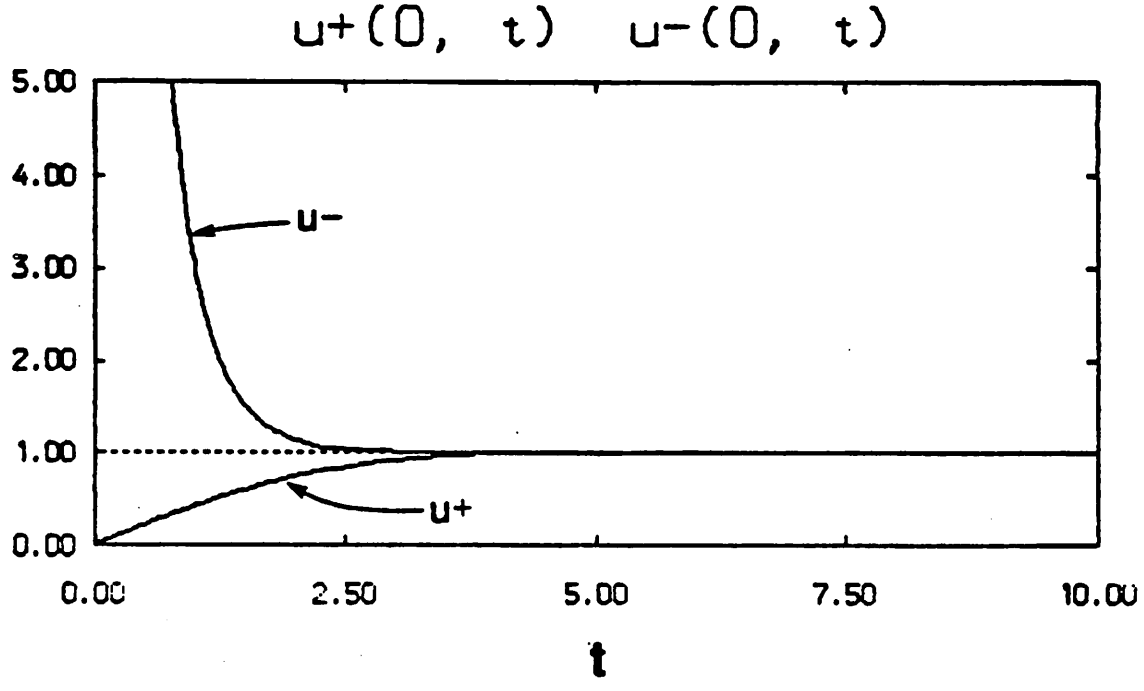

Figure 4(b)

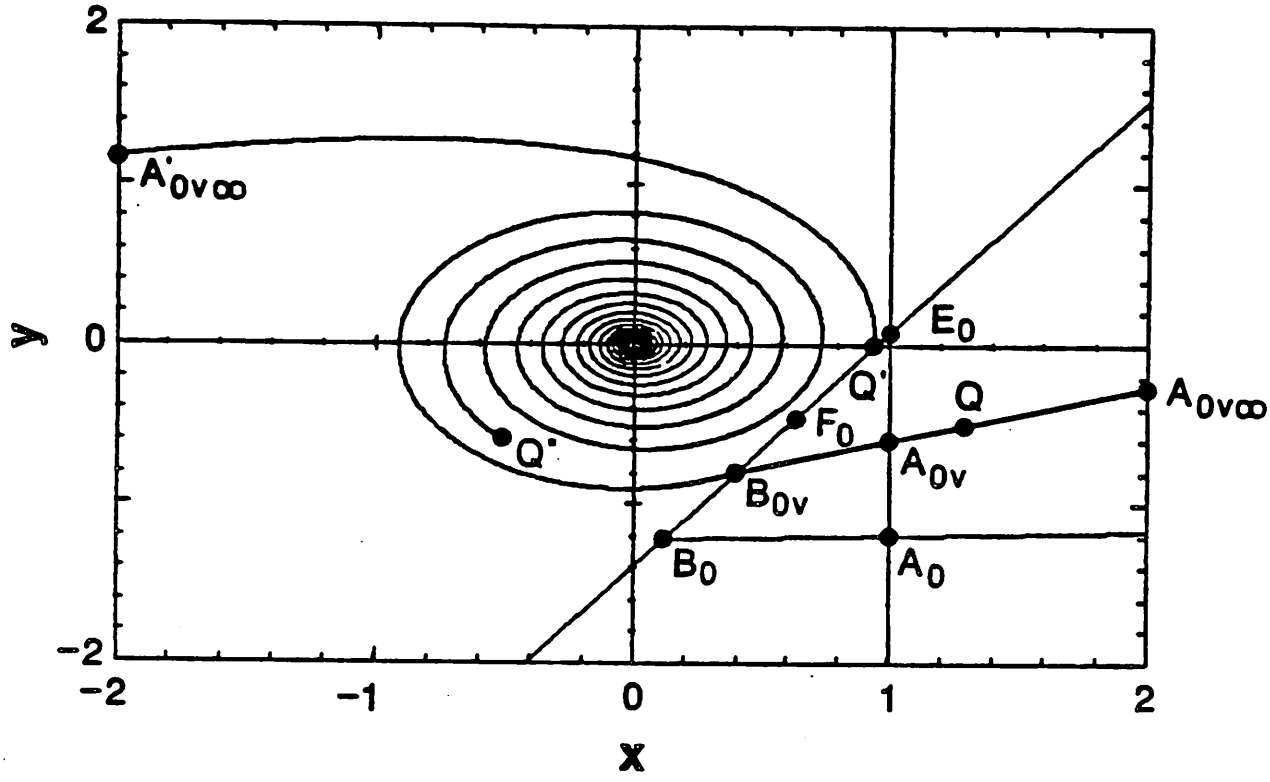

Figure 5(a)

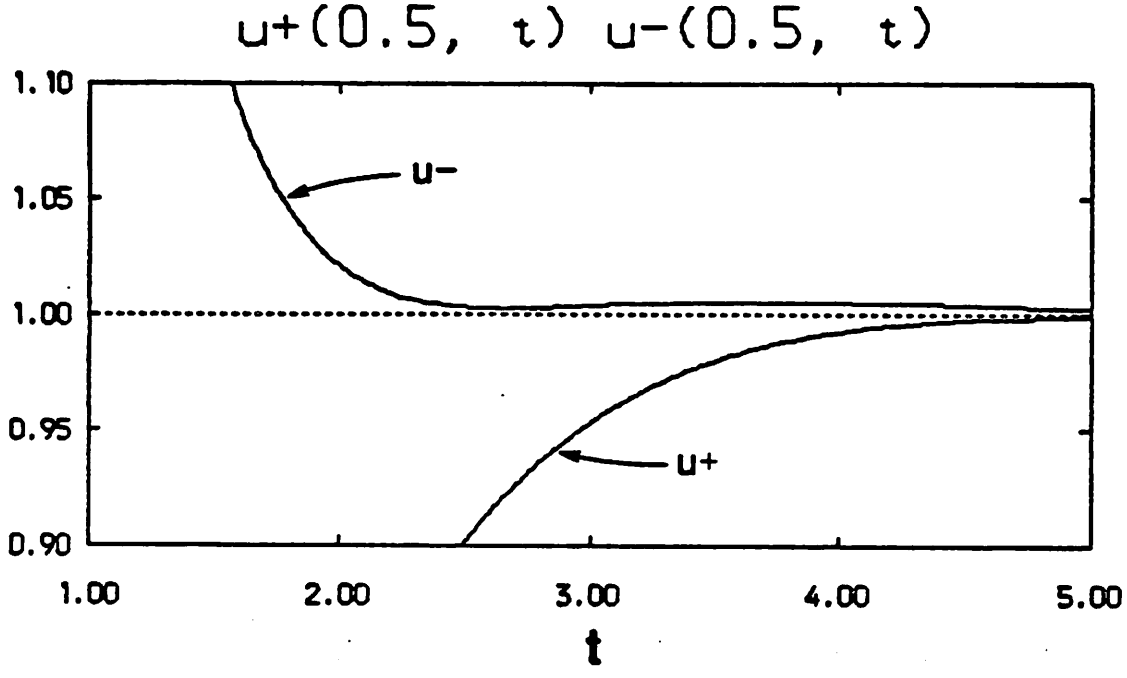

Figure 5(b)

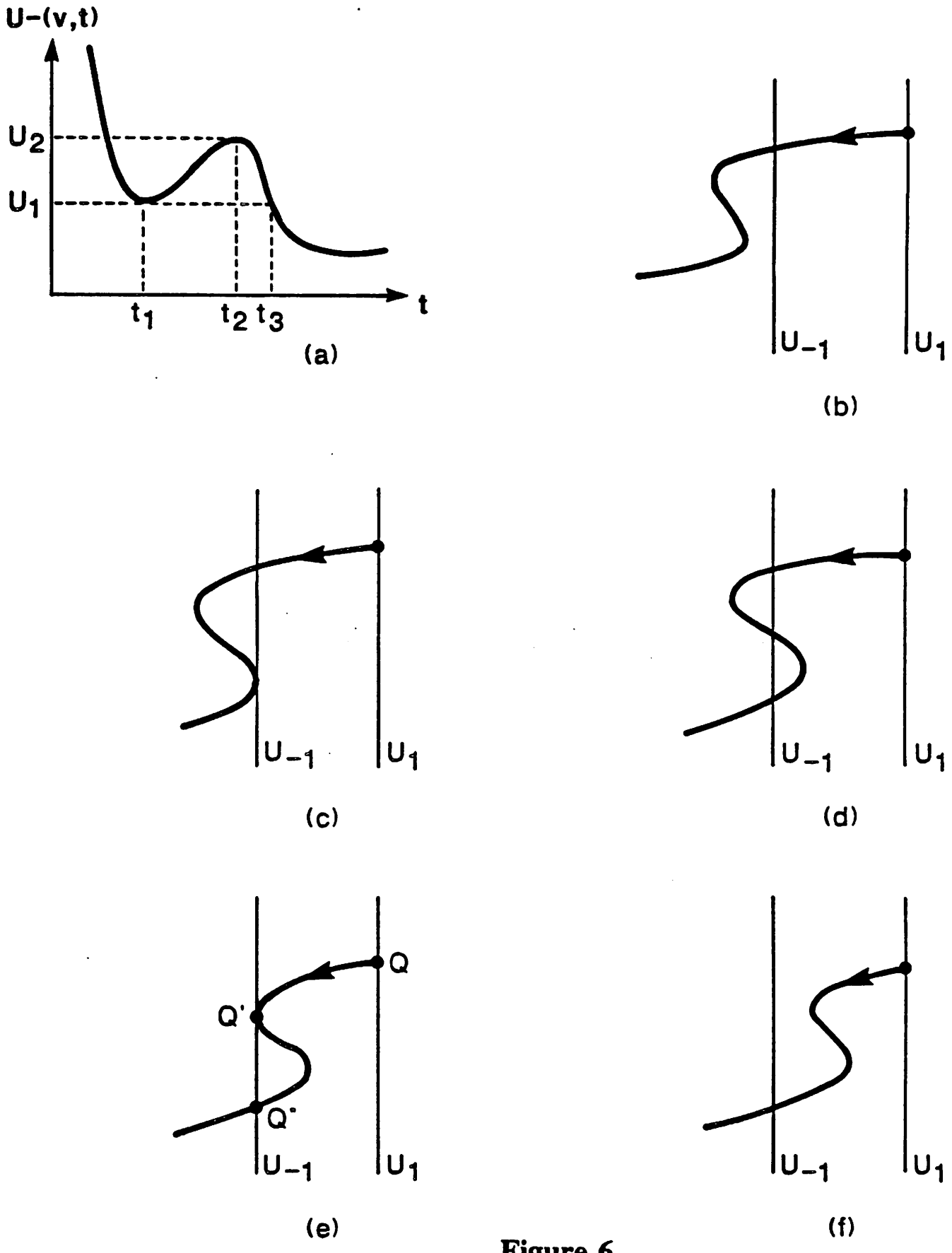

Figure 6

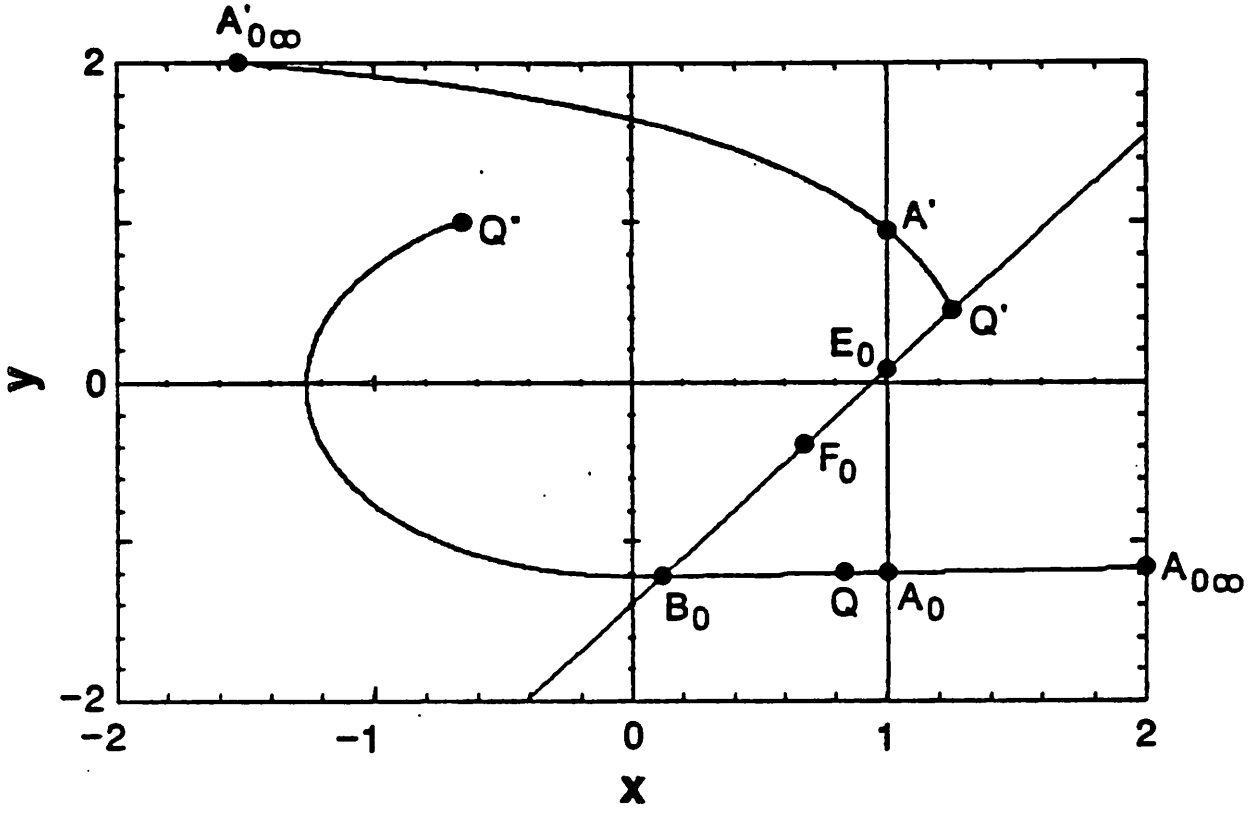

Figure 7(a)

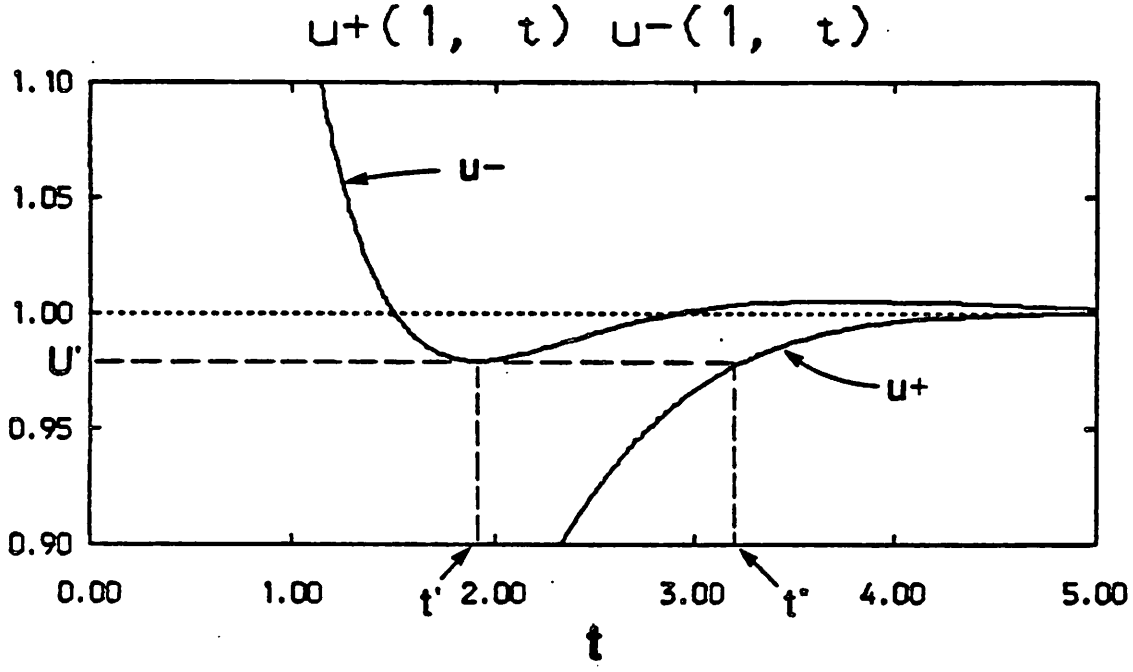

Figure 7(b)

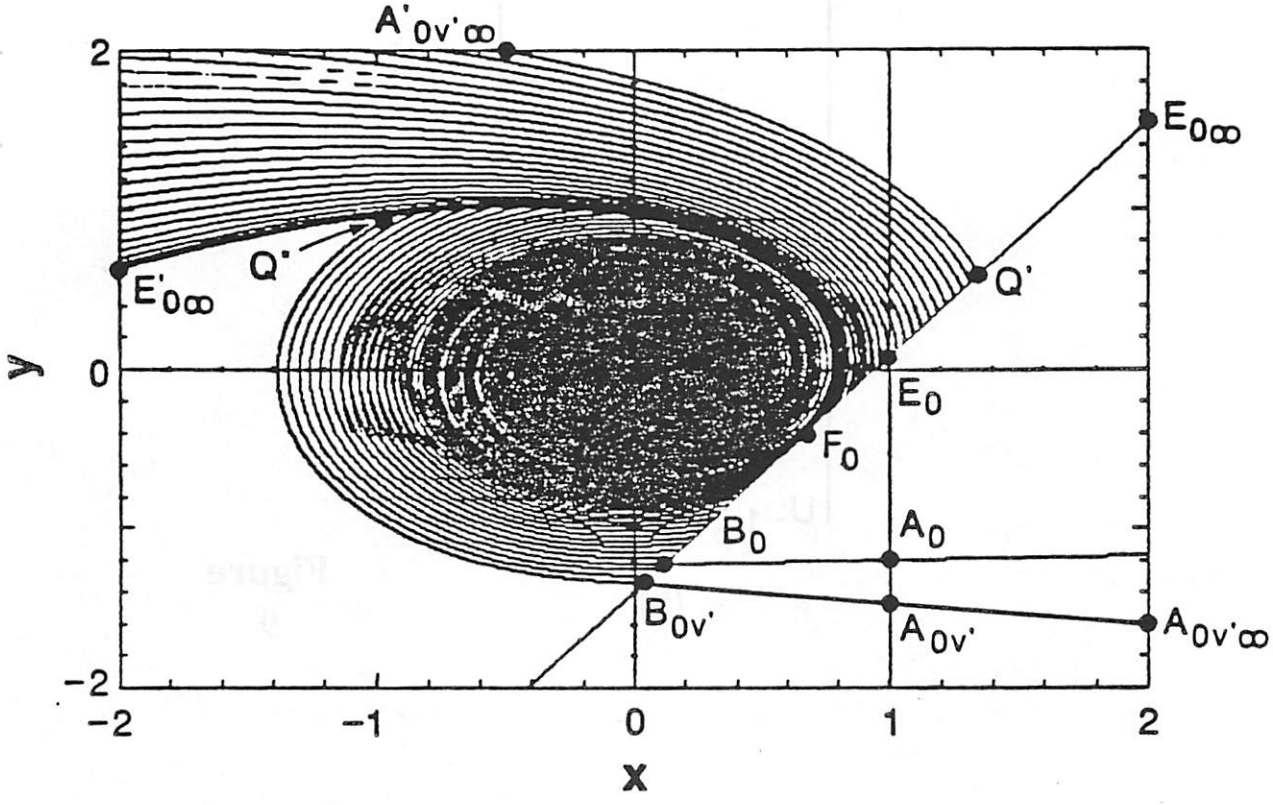

Figure 8

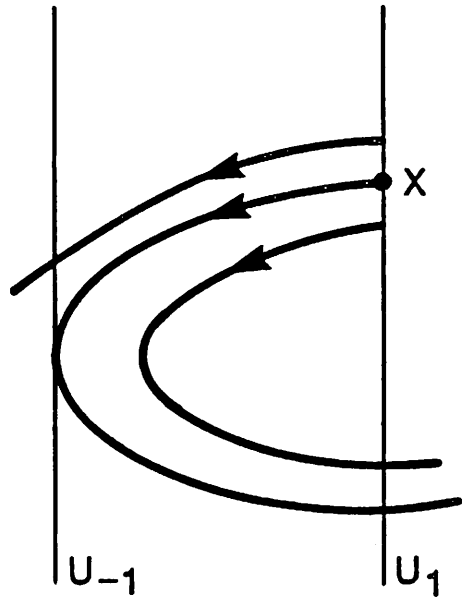

(a)

Figure 9

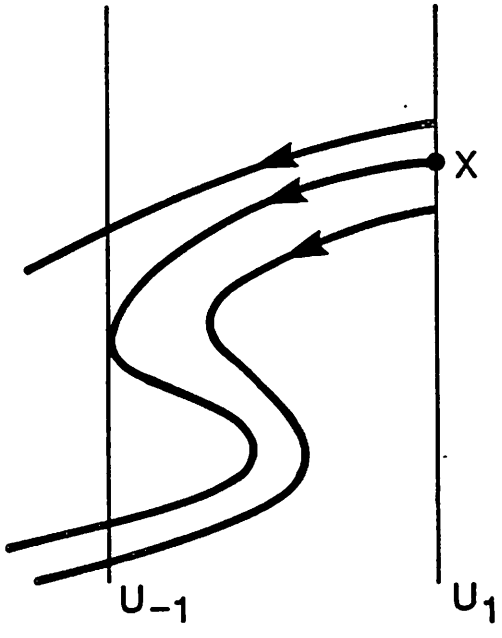

(b)

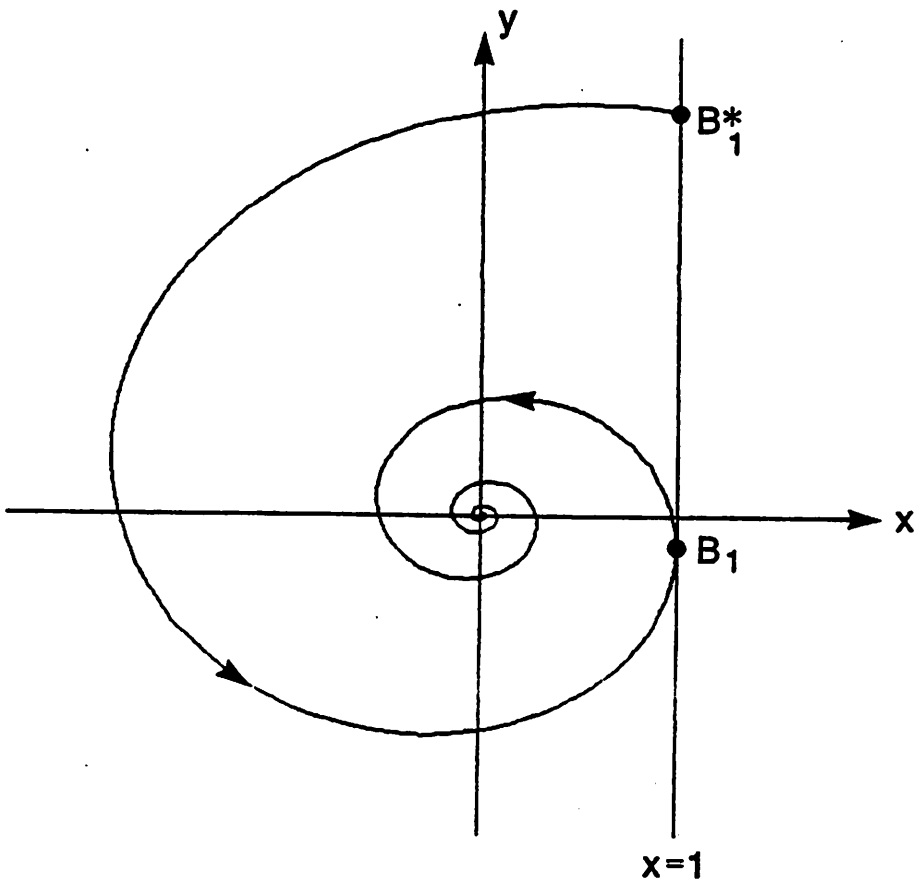

Figure 10

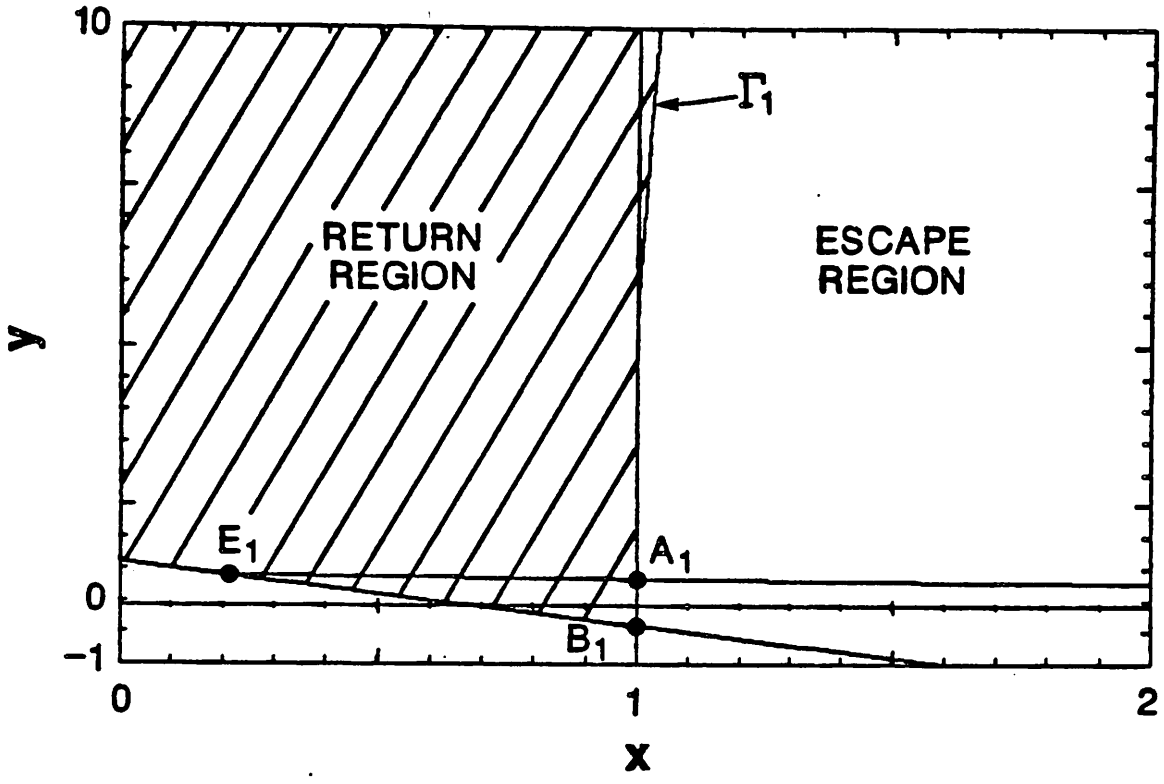

Figure 11(a)

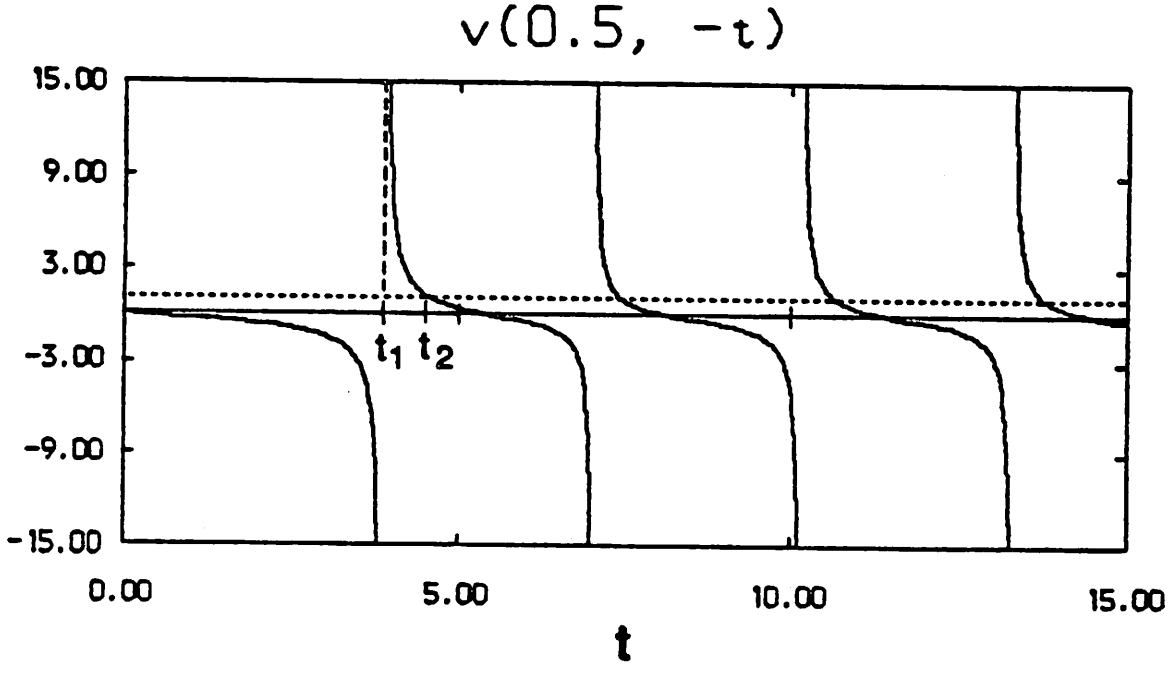

Figure 11(b)

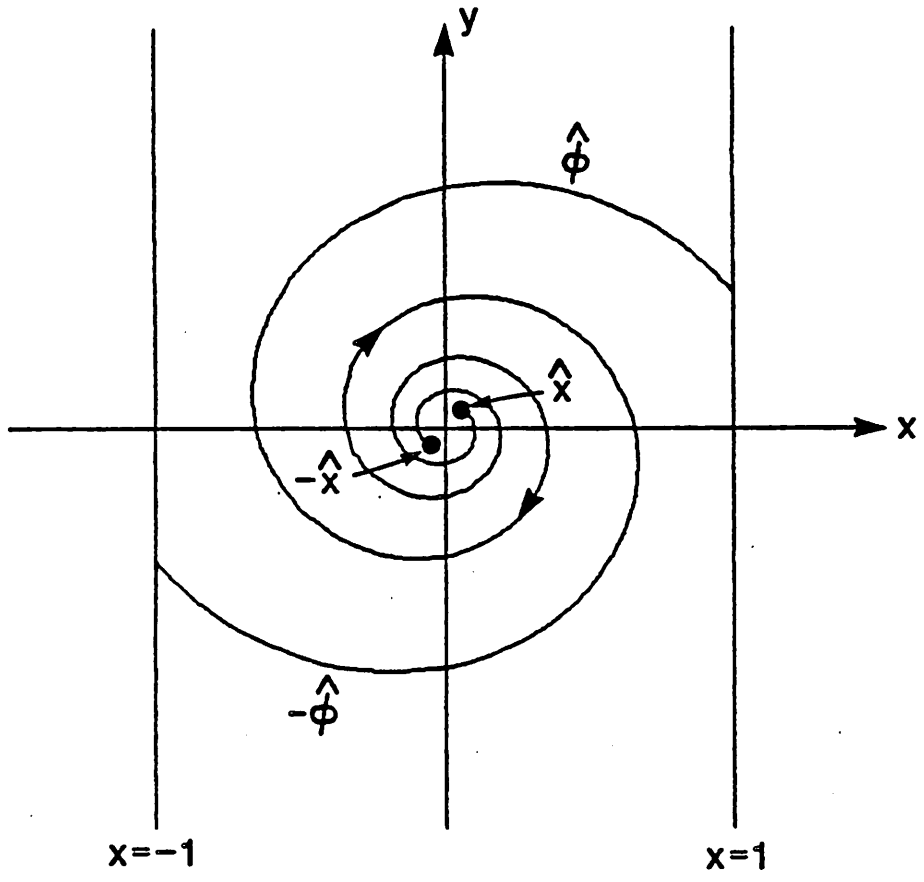

Figure 12

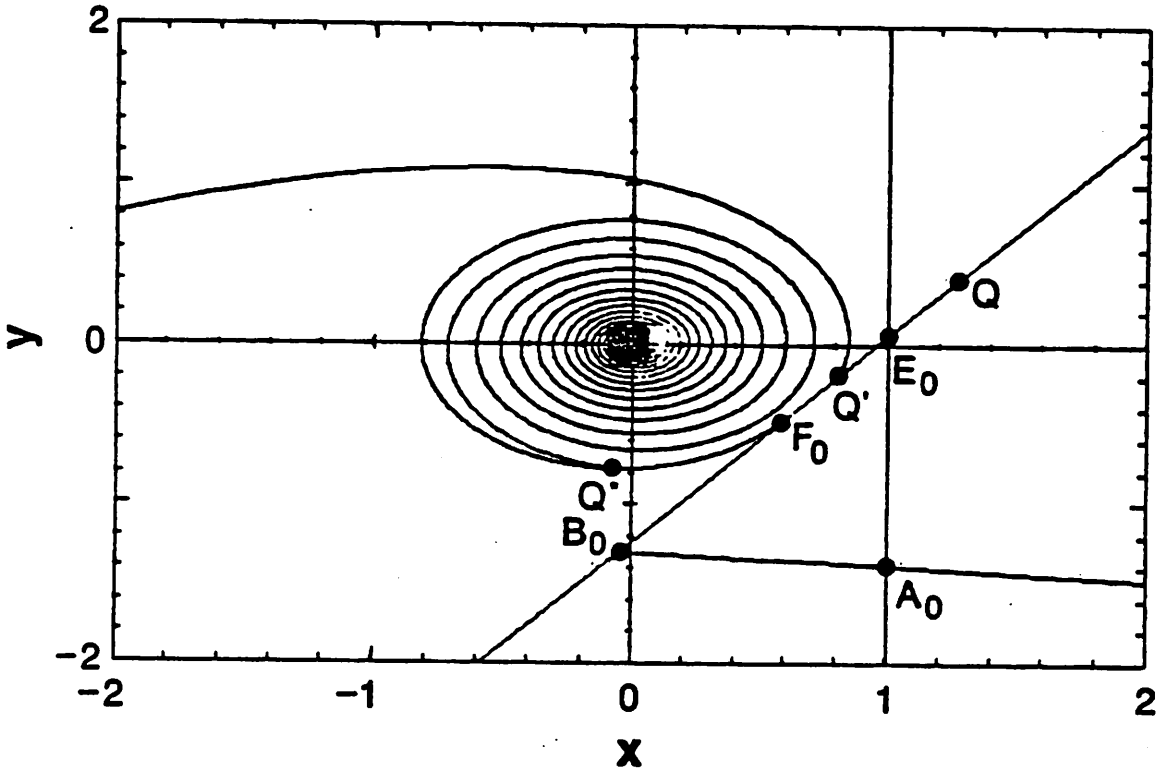

Figure 13(a)

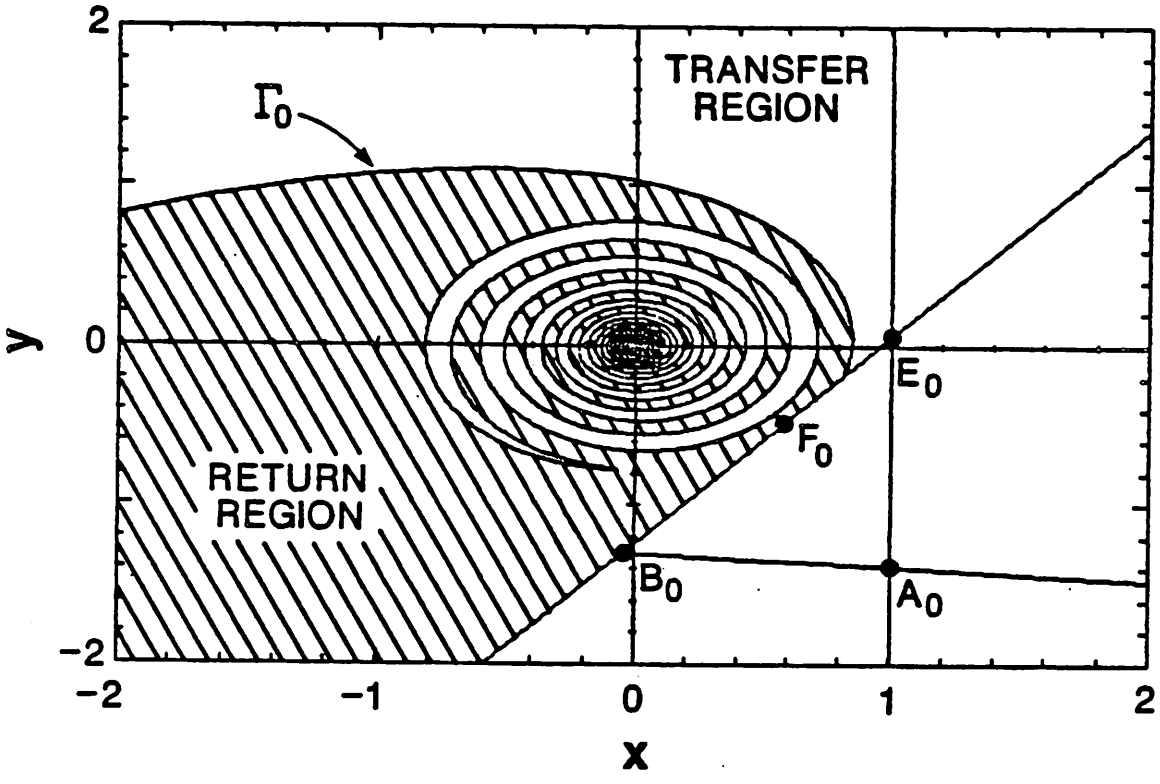
2
0
−2
−2
−1
0
1
2
y
x
Γ_0
TRANSFER
REGION
RETURN
REGION
E_0
F_0
B_0
A_0

Figure 13(b)

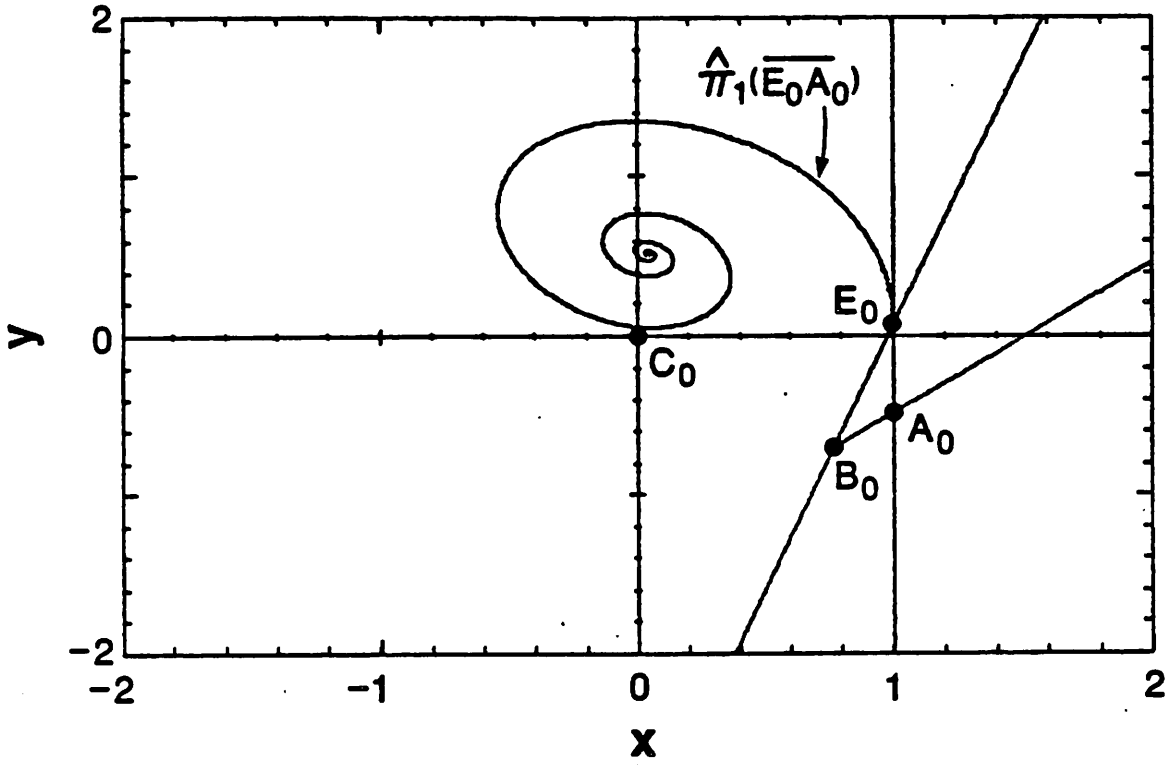

Figure 14(a)

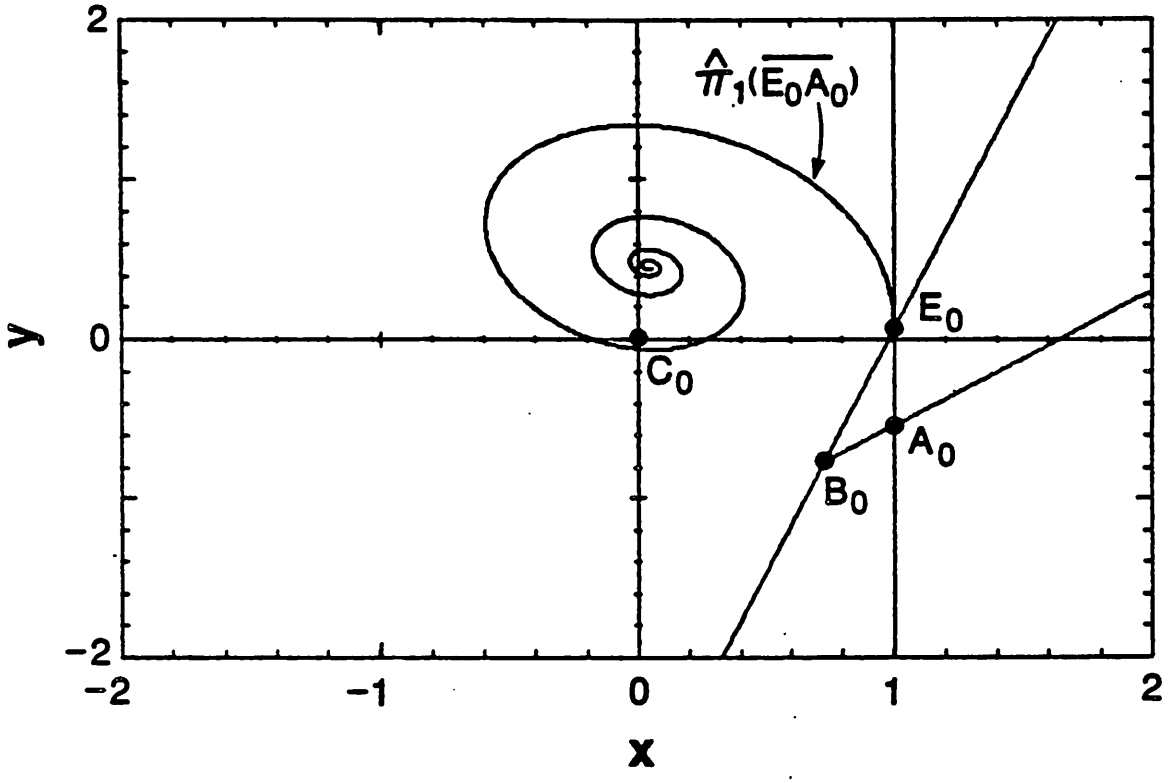

Figure 14(b)

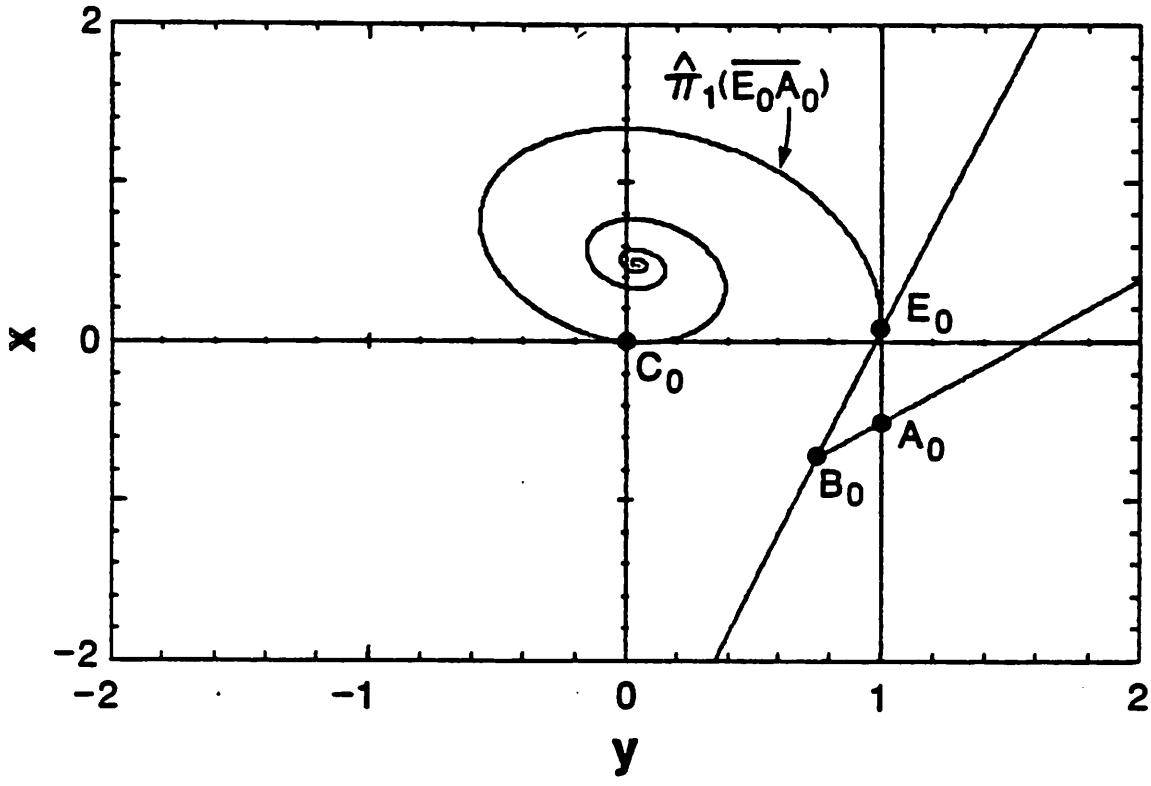

Figure 14(c)

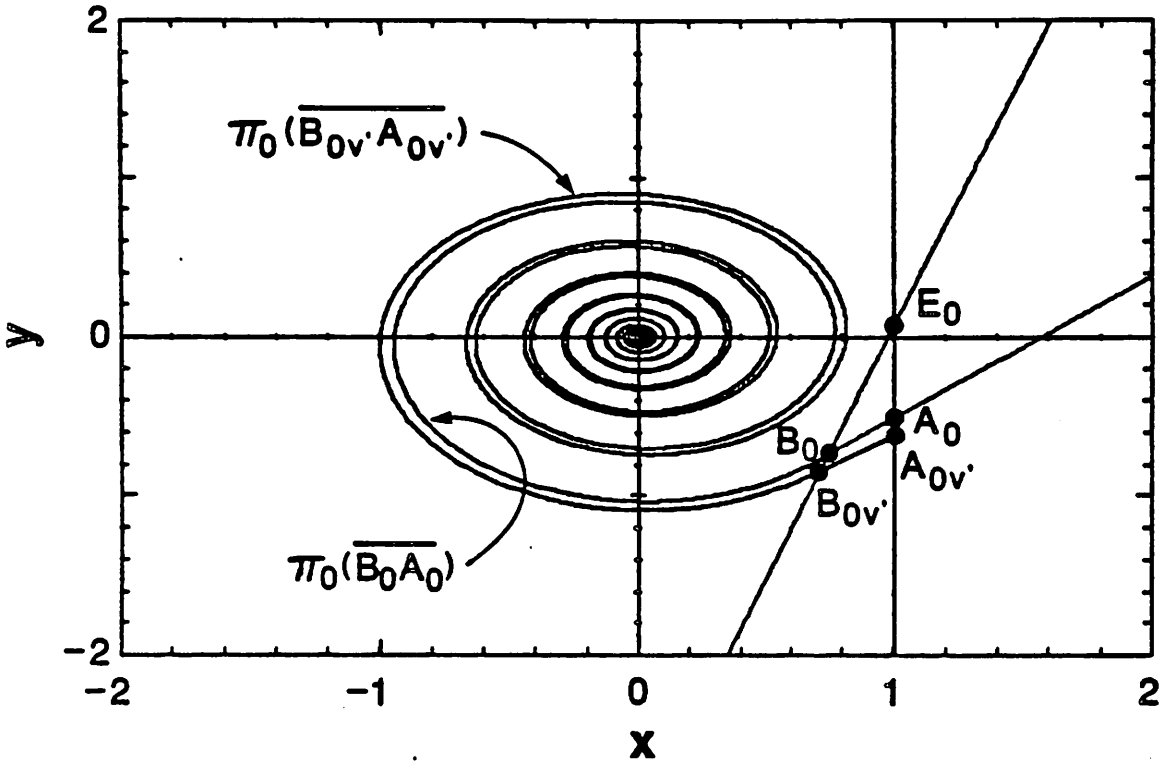
2
0
−2
−2
−1
0
1
2
y
x
$\pi_0(\overline{B_{0v'}A_{0v'}})$
$\pi_0(\overline{B_0A_0})$
E_0
A_0
$A_{0v'}$
B_0
$B_{0v'}$

Figure 14(d)

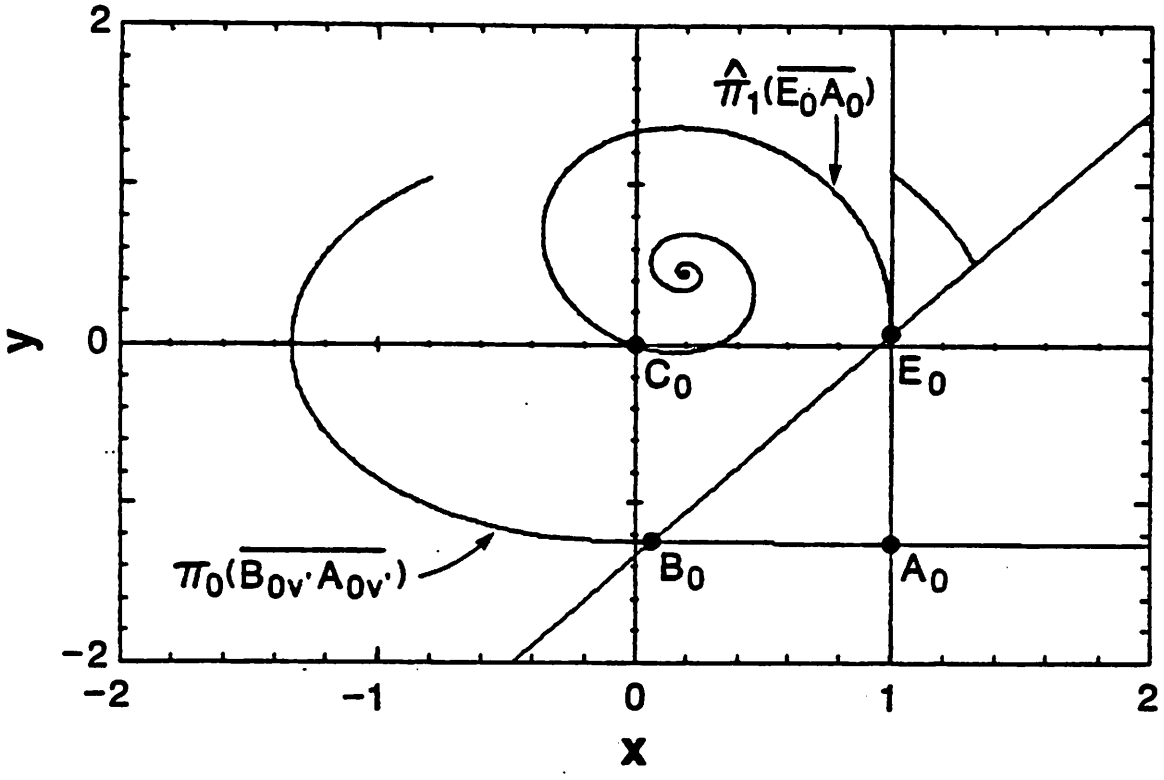
2
0
−2
−2
−1
0
1
2
x
y
$\hat{\pi}_1(\overline{E_0A_0})$
C_0
E_0
B_0
A_0
$\pi_0(\overline{B_{0v'}A_{0v'}})$

Figure 15

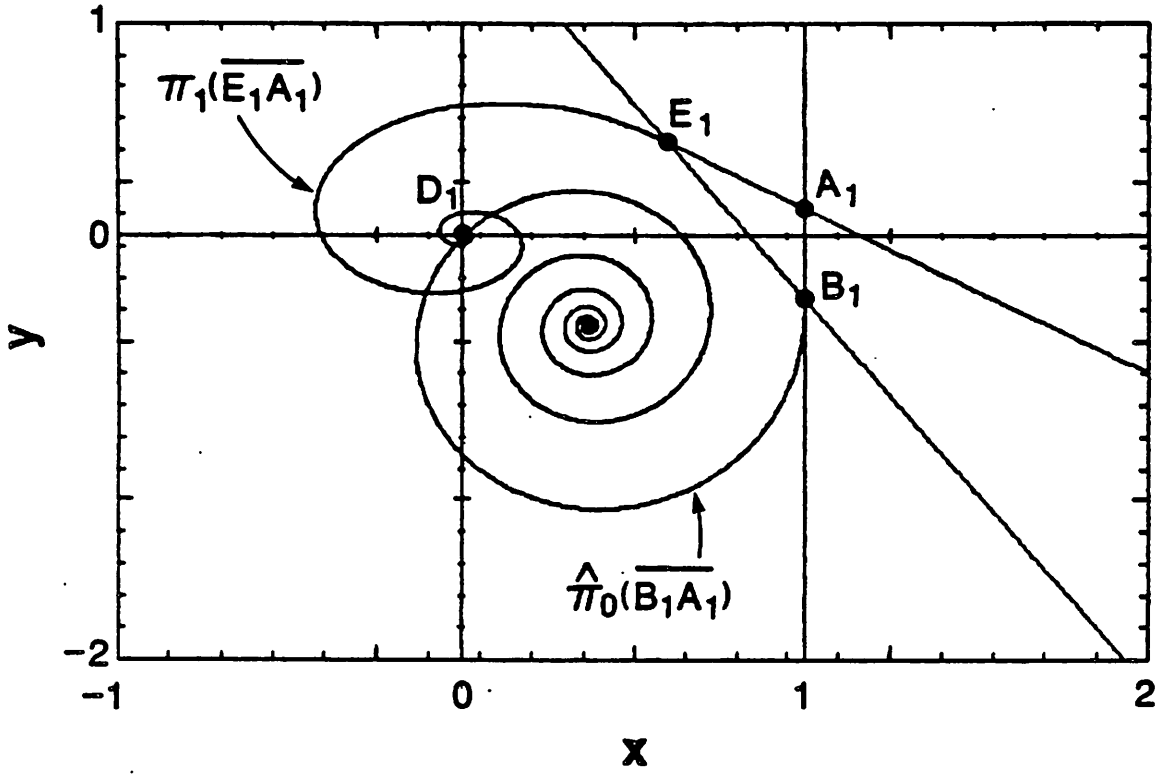
1
0
−2
−1
0
1
2
x
y
$\pi_1(\overline{E_1A_1})$
E_1
D_1
A_1
B_1
$\hat{\pi}_0(\overline{B_1A_1})$

Figure 16(a)

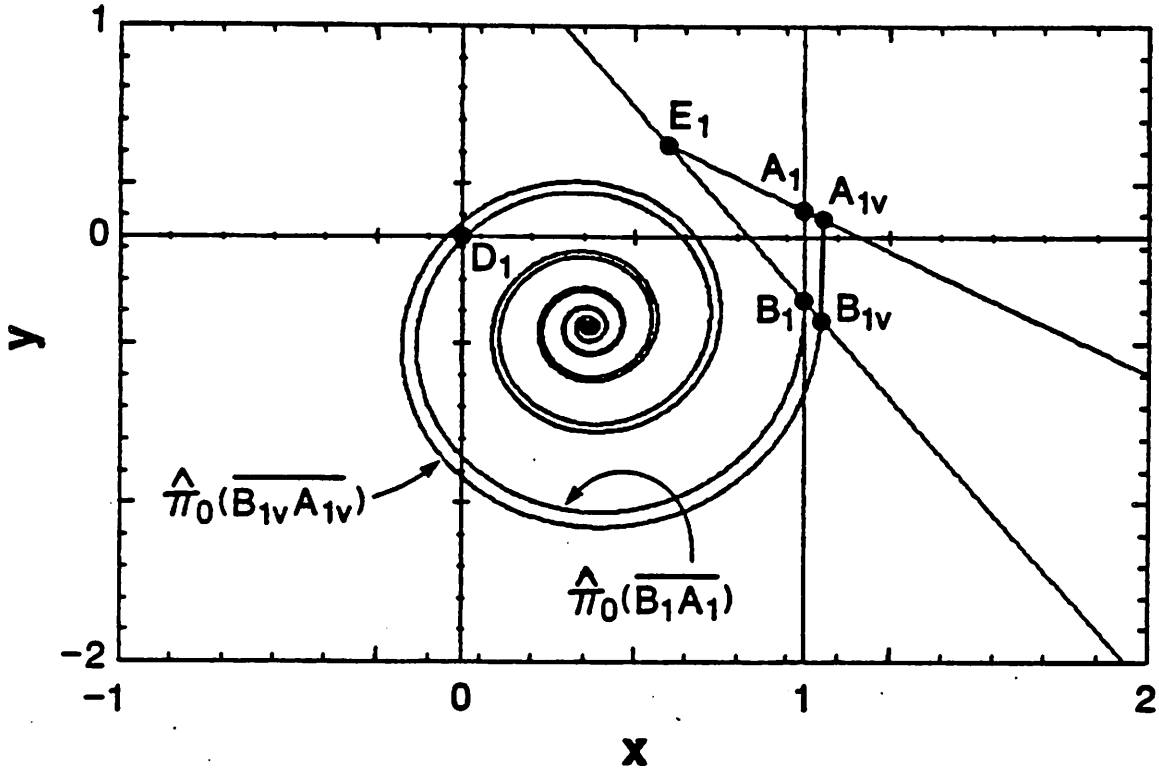
1
0
−2
−1
0
1
2
x
y
E1
A1
A1v
D1
B1
B1v
$\hat{\pi}_0(\overline{B_{1v}A_{1v}})$
$\hat{\pi}_0(\overline{B_1A_1})$

Figure 16(b)

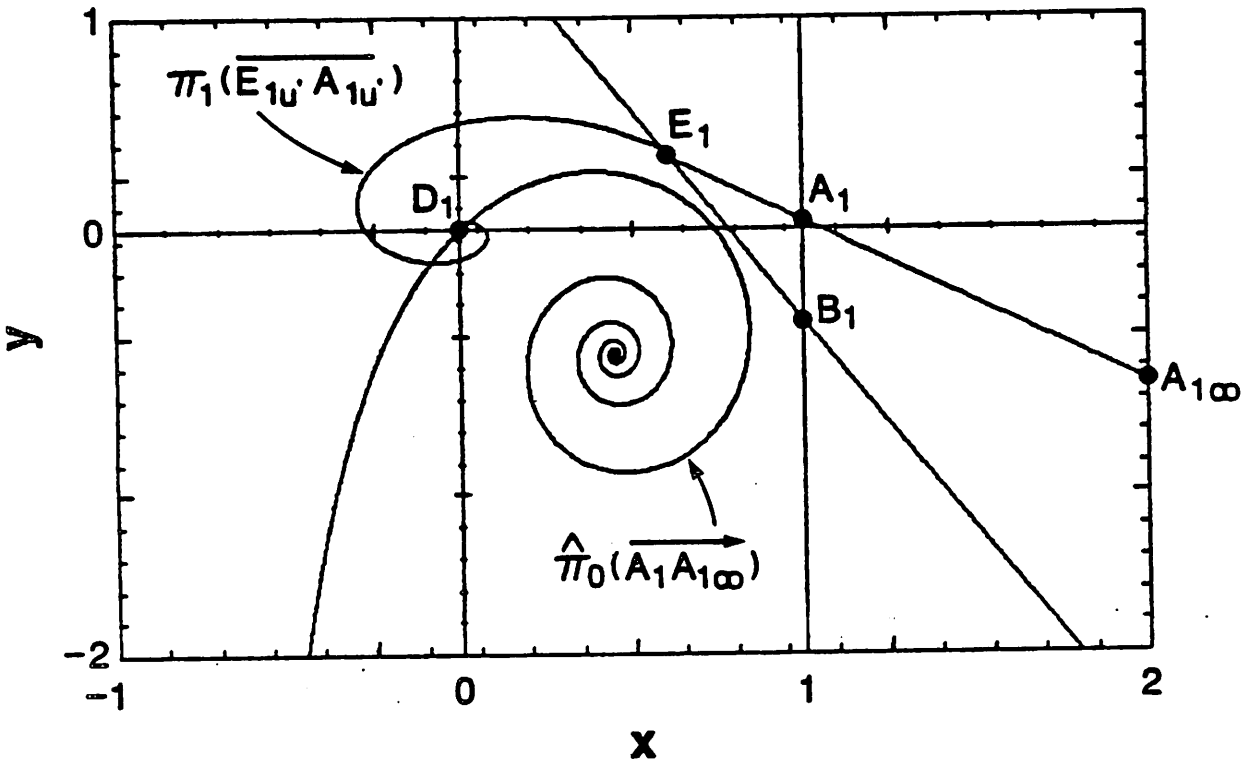
1
0
−2
−1
0
1
2
x
y
$\pi_1(\overline{E_{1u'}A_{1u'}})$
E_1
D_1
A_1
B_1
$A_{1\infty}$
$\hat{\pi}_0(\overrightarrow{A_1A_{1\infty}})$

Figure 17

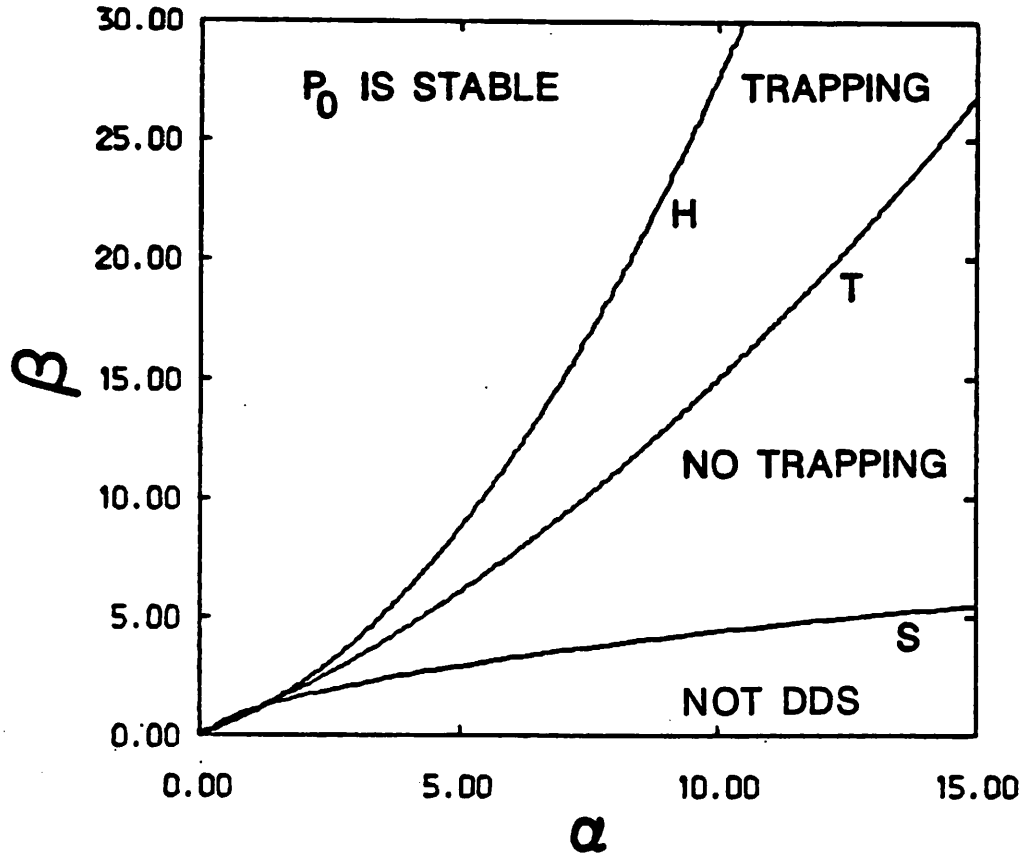
30.00
25.00
20.00
15.00
10.00
5.00
0.00
β
0.00
5.00
10.00
15.00
α
P0 IS STABLE
TRAPPING
H
T
NO TRAPPING
S
NOT DDS

Figure 18(a)

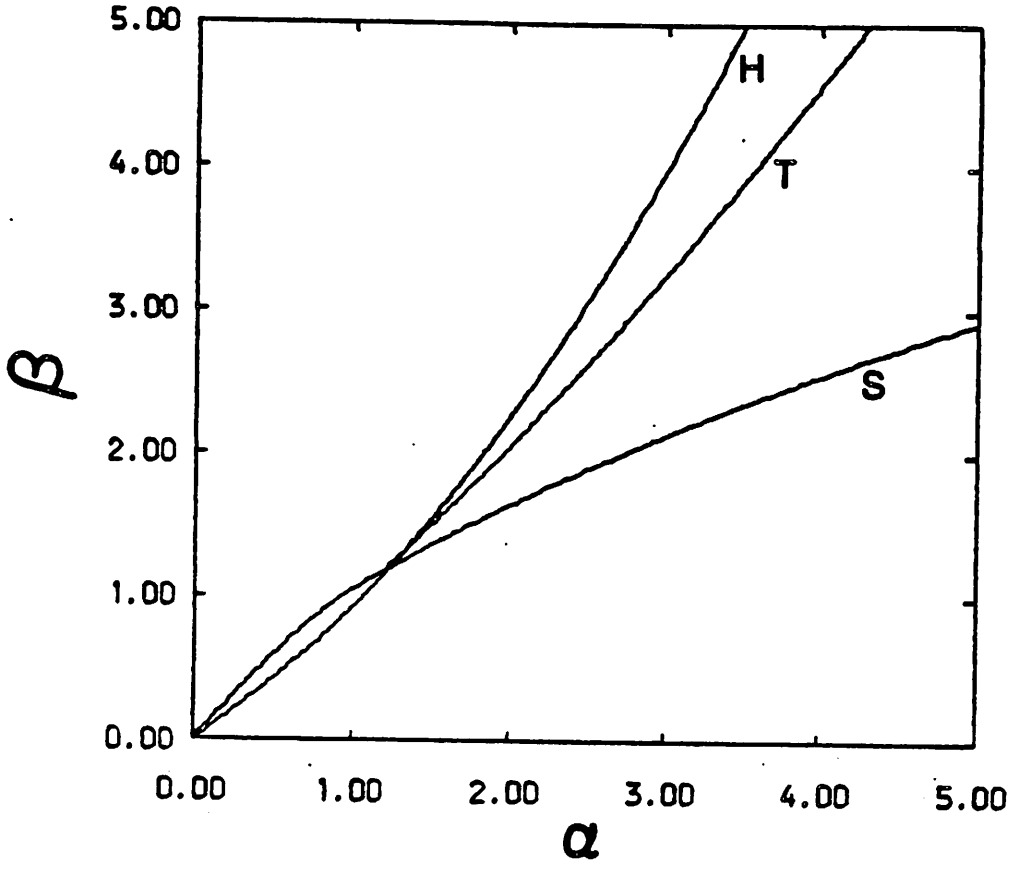

Figure 18(b)

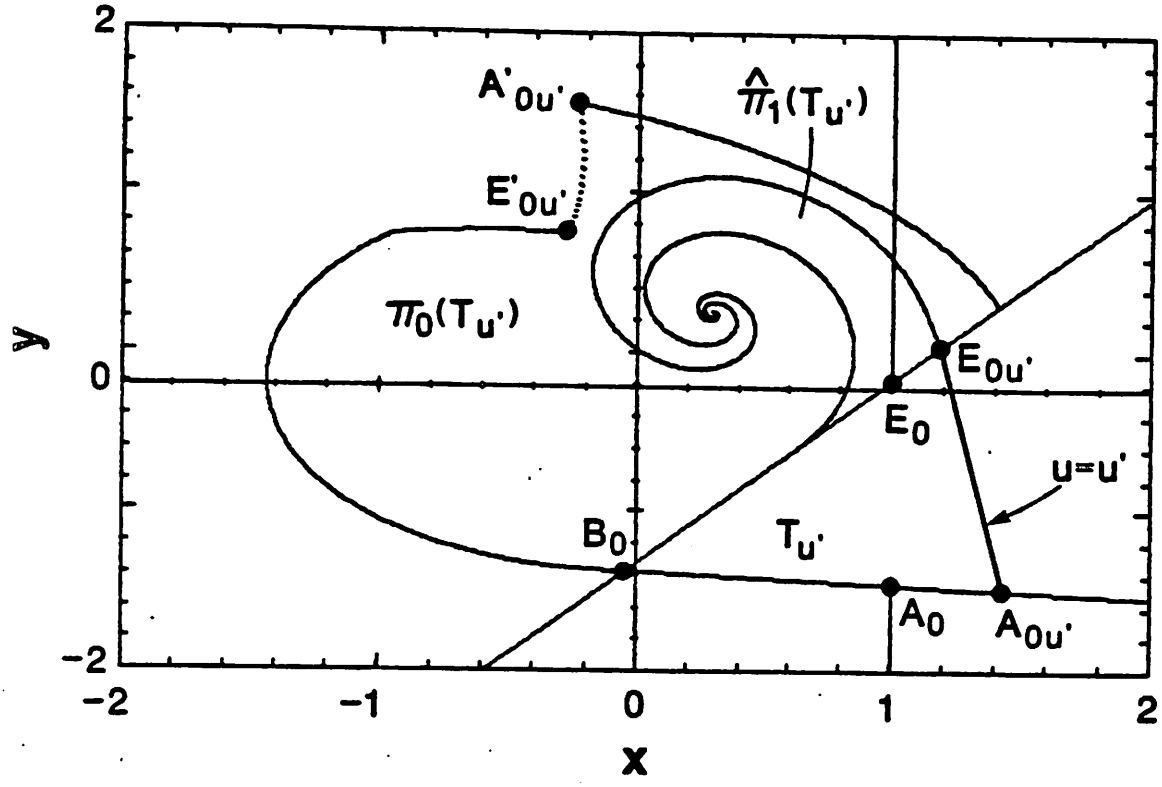

Figure 19

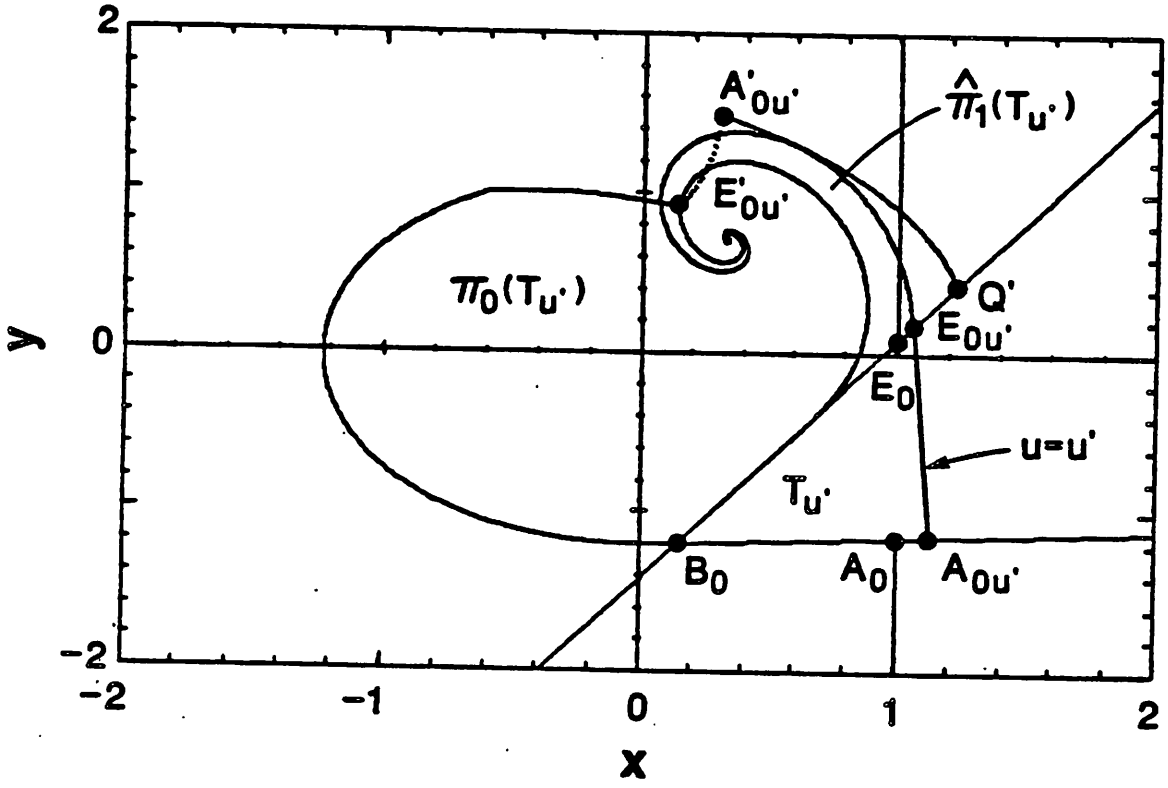

Figure 20(a)

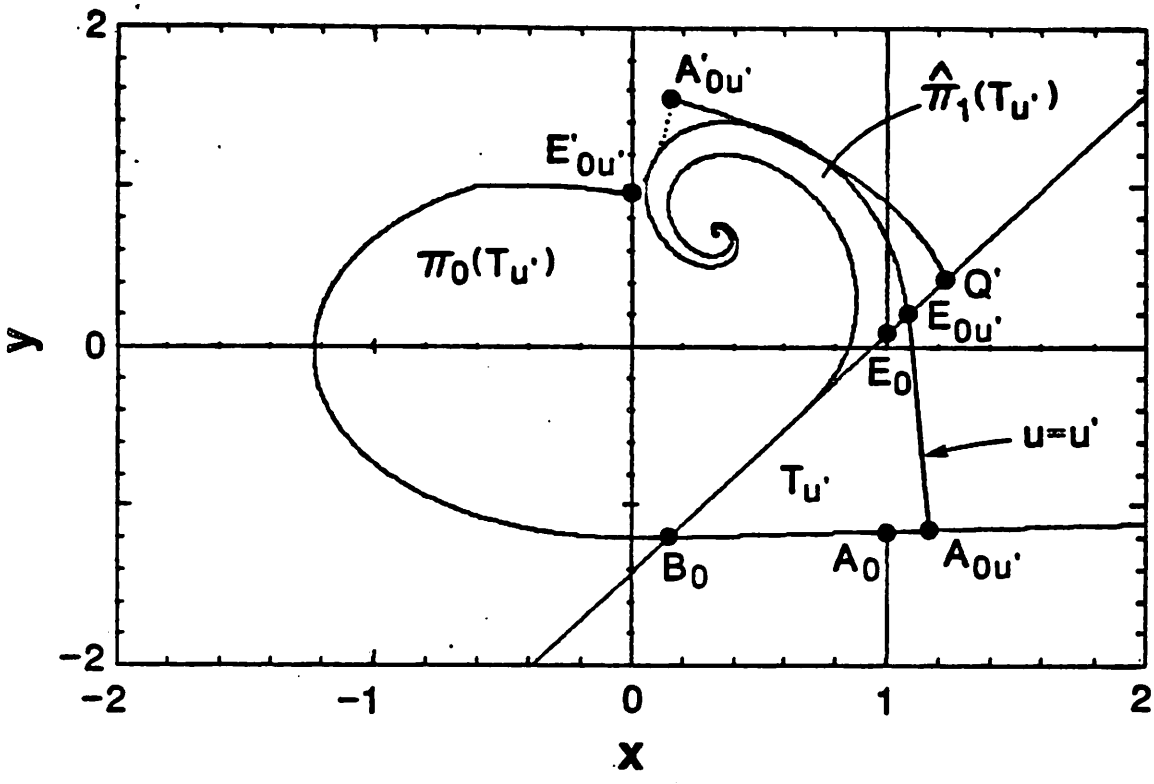

Figure 20(b)

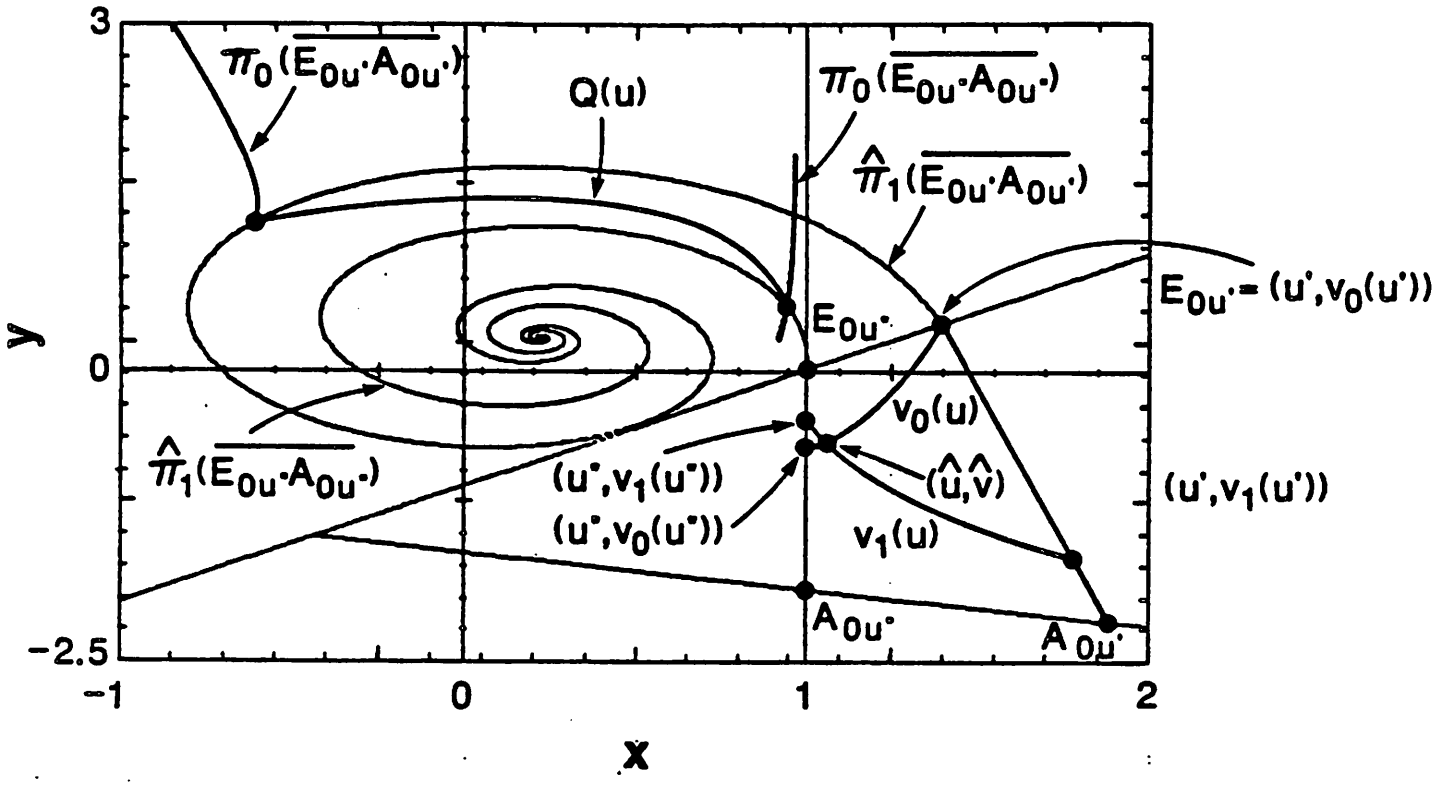
3
0
-2.5
-1
0
1
2
x
y
$\pi_0(\overline{E_{0u}\cdot A_{0u}\cdot})$
Q(u)
$\pi_0(\overline{E_{0u}\cdot A_{0u}\cdot})$
$\hat{\pi}_1(\overline{E_{0u}\cdot A_{0u}\cdot})$
$E_{0u}\cdot = (u', v_0(u'))$
$E_{0u}\cdot$
$v_0(u)$
$\hat{\pi}_1(\overline{E_{0u}\cdot A_{0u}\cdot})$
$(u^*, v_1(u^*))$
$(u^*, v_0(u^*))$
$(\hat{u}, \hat{v})$
$(u', v_1(u'))$
$v_1(u)$
$A_{0u}\cdot$
$A_{0u}\cdot$

Figure 21